A continuous 100 thousand-year stalagmite $\delta^{18}O$ record from the Yucatan Peninsula: implications for Caribbean hydroclimate on orbital and millennial timescales

by

Morgan Laine Hill

A thesis submitted to the Graduate Faculty of
Auburn University
in partial fulfillment of the
requirements for the Degree of
Master of Science in Geology

Auburn, Alabama
May 5, 2019

Approved by

Dr. Martín Medina-Elizalde, Chair, Associate Professor of Geosciences
Dr. Ming-Kuo Lee, Robert B. Cook Professor and Department Chair of Geosciences
Dr. Matthew Waters, Assistant Professor of Crop, Soil and Environmental Sciences

Table of Contents

Abstract

I present a new stalagmite $\delta^{18}O$ record, named Katún, collected from Río Secreto Natural Reserve in the Yucatan Peninsula (YP) that spans the interval between 198 kyr to 320 kyr before present (BP), thus offering the oldest continuous paleoclimate record from the tropical Americas. The Katún $\delta^{18}O$ record is interpreted to reflect precipitation amount based on modern observations and isotopic equilibrium calculations. On orbital timescales, the Katún $\delta^{18}O$ record shows the general features observed in atmospheric CO_2, tropical SSTs, and benthic foraminiferal $\delta^{18}O$ records. Specifically, marine isotope stages (MIS) 7, 8, and 9 are readily identifiable in the stalagmite $\delta^{18}O$ record. The Katún $\delta^{18}O$ record suggests humid conditions and low amplitude precipitation variability during MIS 7 and 9 interglacial intervals, coeval with high tropical sea surface temperatures (SST) and high atmospheric CO_2. During glacial inceptions after MIS 9 and 7, the Katún $\delta^{18}O$ record suggests high amplitude precipitation variability and an increase in the frequency and intensity of drought events. Dominant periodicities between 4-8 kyr in the Katún $\delta^{18}O$ record resemble millennial scale climate variability seen in Greenland ice core $\delta^{18}O$ records from the last glacial. We suggest that glacial-interglacial precipitation variability in the broad Caribbean region reflects atmospheric greenhouse forcing via its effect on tropical Atlantic SST variability. In addition, we propose that Caribbean precipitation on millennial timescales reflects shifts in the intensity and position of the Intertropical Convergence Zone (ITCZ) in association with Atlantic Meridional Overturning Circulation (AMOC) changes, as hypothesized for the last glacial interval.

Acknowledgments

I would first like to acknowledge my deepest gratitude to the chair of my advising committee, Dr. Martín Medina-Elizalde, for his endless supply of knowledge, patience, enthusiasm, and support. I could not have made it this far without your invaluable mentorship and encouragement. I'd also like to thank Jill and the rest of your family for being so kind and hospitable. I feel like I have become a part of the family, something I couldn't be more grateful for.

I would also like to thank my additional committee members Dr. Ming-Kou Lee and Dr. Matthew Waters who generously gave their time, advice, and criticisms. A big thank you to Dr. Matthew DeCesare for the amount of lab work you contributed to this project and for being a great buddy in Mexico. Also, thank you to Dr. Josué Polanco-Martínez who tirelessly helped me out with the numerous analyses this project required.

Thank you to Dr. Sandy Ebersole who provided critical mentorship throughout the years. I would not have accomplished all I have if it weren't for you.

I'd also like to thank my family and friends for being the greatest support system in the world. I love you and I cannot thank you enough for consistently being there for me.

Lastly, a blanket thank you to the Auburn University Geosciences faculty, staff, and students. Collectively, you have a close-knit, supportive, department that provides a welcoming, inclusive environment for all. The plains will always feel like home because of you all. Thank you to all of the invaluable friendships I've made during my time at Auburn. This experience would not have been the same without you.

List of Tables

List of Figures

List of Abbreviations

AMO	Atlantic Multidecadal Oscillation
AMOC	Atlantic Meridional Overturning Circulation
BP	before present
CB	Cariaco Basin
CLLJ	Caribbean low-level jet
CO_2	carbon dioxide
D-O	Dansgaard-Oeschger
ENSO	El Niño-Southern Oscillation
GCM	general circulation model
GHG	greenhouse gas
HISPEC	High-Precision Mass Spectrometry and Environment Change Laboratory
ITCZ	Intertropical convergence zone
kyr	thousand years
LGM	Last Glacial Maximum
MC-ICP-MS	multi-collector inductively coupled plasma mass spectrometer

MIS	marine isotope stage
RS	Río Secreto
SD	standard deviation
SST	sea surface temperature
YP	Yucatan Peninsula

1. Introduction

This study seeks to characterize the magnitude and frequency of hydroclimate variability in the Yucatan Peninsula (YP), Mexico, over a 100,000-year (kyr) time interval between 320 and 198 kyr BP. Climatologically, the correlation between precipitation variability in the YP and that observed in the larger Caribbean and Gulf of Mexico regions today indicates a coherent hydrological sensitivity of these regions to factors operating on large spatial scales (Fig. 1). The YP, positioned between latitudes 18°N and 21°N, experiences seasonal monsoonal precipitation cycles with up to 80% of annual precipitation occurring between the June-October rainy season (CONAGUA, 2012; Medina-Elizalde et al., 2016b) and a distinctive annual cycle of precipitation characterized by the Nortes, Dry and Rainy seasons. The Nortes cold front season occurs between the months of November and February, the Dry season during March-April-May and the Rainy season between June and October. The Rainy season, also known as the hurricane season, has a bimodal distribution of precipitation with maxima during June and September and a precipitation drop by July and August, known as the midsummer drought (Magaña et al., 1999). Precipitation maxima in the YP occur during the months of September when the ITCZ reaches its northernmost distribution and when the peninsula experiences the maximum tropical cyclone frequency. Studies with regional models and the NCEP-NCAR Global reanalysis indicate that the dominant source of moisture for the YP is the Caribbean Sea and is linked to the Caribbean Low-Level Jet (CLLJ; Karmalkar et al., 2011; Mestas-Nuñez et al., 2007; Munoz et al., 2008; Vuille et al., 2003). Another source of moisture, which can dominate the seasonal and annual budget of precipitation in the northern Caribbean region, is provided by tropical waves and cyclones. Instrumental cyclone data indicates that the short-lived precipitation fluxes from cyclones can contribute up to 20% of western North Atlantic cumulative rainfall, including along

the US Gulf and Mexican coasts (Larson et al., 2005). Precipitation processes for the YP have been characterized for the last glacial maximum (LGM) and Holocene and show the YP experiences a strong seasonality in precipitation which makes it an ideal location to reconstruct precipitation using oxygen isotopes from speleothems (cave carbonate deposits) (Medina-Elizalde et al., 2016b).

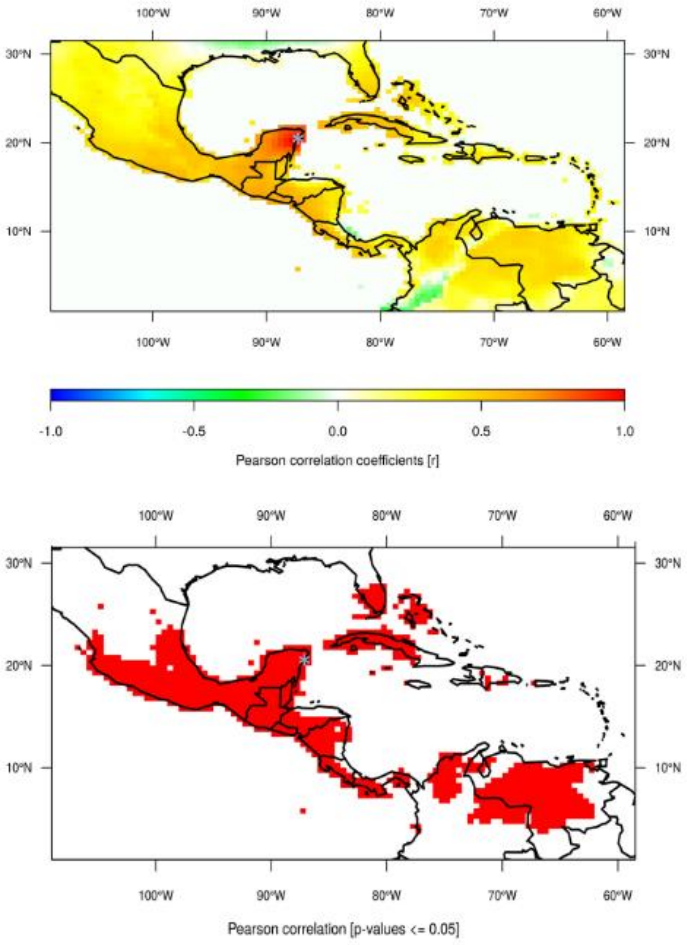

Figure 1) Spatio-temporal correlation analysis of precipitation (monthly values from 01/1901 to 12/2013 and with a spatial coverage of 0.5° latitude by 0.5° longitude) at the location (20°15′N, 87°45′W) (close to Playa del Carmen, Yucatan, Mexico). Location of Rio Secreto indicated with light blue asterisk. The precipitation data set comes from the GPCC Global Precipitation Climatology Centre and is available from https://www.esrl.noaa.gov/psd/data/gridded/data.gpcc.html. From Medina-Elizalde et al. (2017).

The YP is a carbonate platform consisting of limestones, dolomites, and evaporites reaching thicknesses of greater than 1,500 m (Weidie, 1985). Exposed ground surface sediment

spans Upper Cretaceous to Holocene in age with gradually younger carbonates deposited towards the peninsula margins (Fig. 2; Lopez-Ramos, 1975; Schönian et al., 2005). Ancient reefs

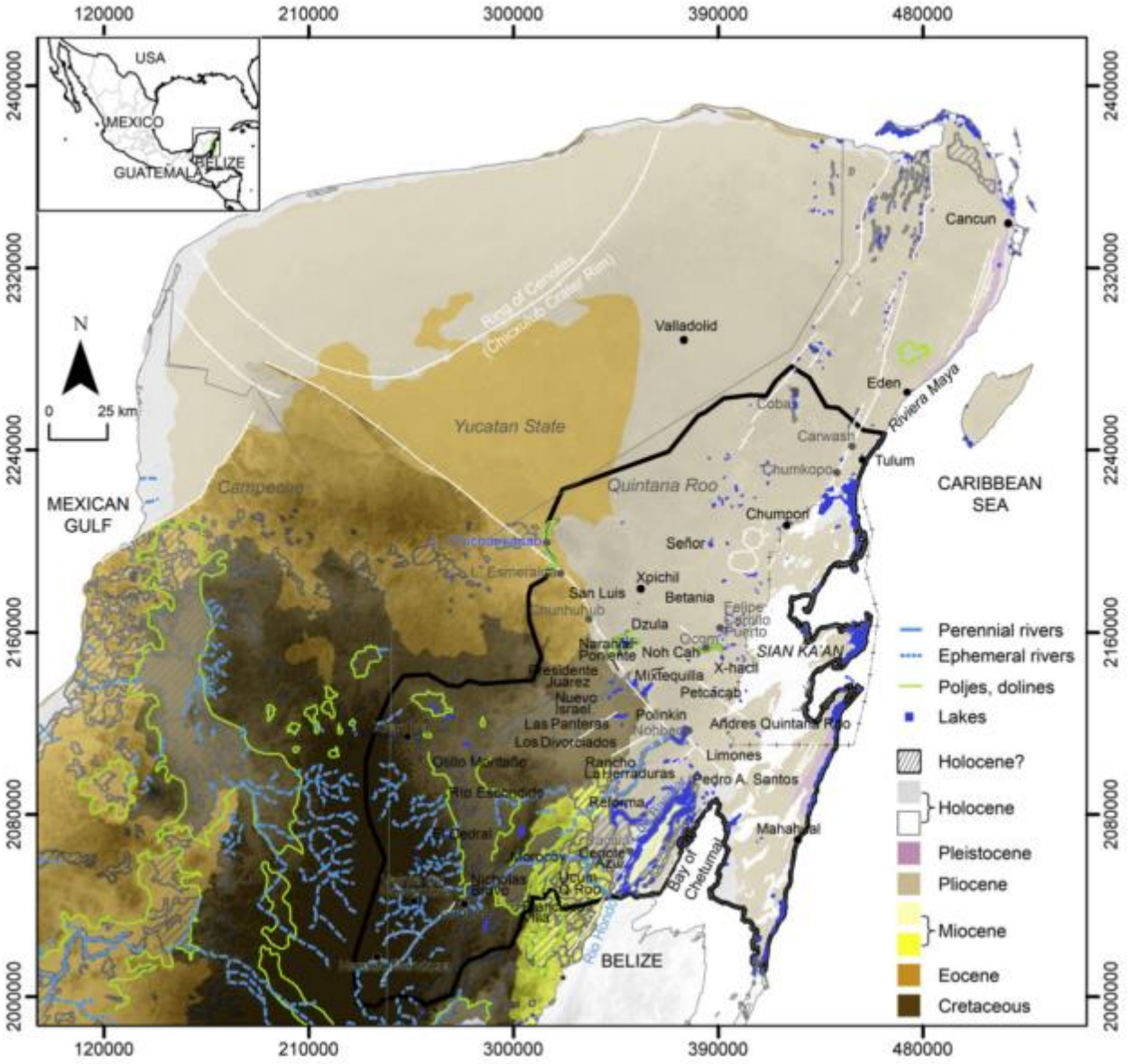

Figure 2) Geology of the Yucatan Peninsula, modified from SGM (2007). Oldest sediments dated as Cretaceous instead of Paleocene, based on Schönian et al. (2005) and Lopez- Ramos (1975) (Ichaiche Formation). Topography from SRTM (USGS, 2006) overlain as grey-scaled transparent. From Gondwe et al., 2010

and bays of the platform (Shaw, 2016) record details of sea level change and the geomorphic responses to it; Quaternary and Holocene sea-level changes are credited for creating vast karst platforms throughout cycles of vadose and phreatic settings. Carbonates in the YP are heavily karstified, hosting abundant caves and cenotes throughout the northern lowlands. Cave morphology and complexity greatly vary within the peninsula with inland systems preferentially dissolving along native fracture zones and coastal systems dominated by dissolution in the freshwater/saline water mixing zone (van Hengstum et al., 2010). Cave development occurred in multiple phases associated with a combination of endogenic and exogenic processes. Cave distribution, vertical development, and the hydrogeologic, structural, and stratigraphic controls of the karst network were influential factors in development of the eastern coast of the YP. Notably, a ring of cenotes surrounds the Chicxulub meteorite impact crater, located on the northwestern coast of the YP with the date of impact coinciding with the Cretaceous-Paleogene boundary (Gondwe et al., 2010).

1.1. Relationship between precipitation amount and $\delta^{18}O$ composition (amount effect)

Climate models with isotope tracers and the IAEA GNIP instrumental database indicate that precipitation $\delta^{18}O$ in the YP is controlled by precipitation amount (i.e. amount effect) on seasonal and interannual time scales (Figs. 3 & 4; Vuille et al., 2003). This implies that if it rains the same amount during five consecutive years, the precipitation $\delta^{18}O$ composition (amount weighted) is expected to remain practically unchanged. If precipitation amount changed during one given year, then precipitation $\delta^{18}O$ would change according to the amount effect relationship. Precipitation estimates from stalagmite $\delta^{18}O$ would thus represent the average precipitation amount of one, two, or the number of years the calcite sample integrates. Because

stalagmite $\delta^{18}O$ is expected to reflect equilibrium with drip water $\delta^{18}O$ and drip water in turn reflects rainfall $\delta^{18}O$ on an annual basis (Lases-Hernández et al., 2018; Lambert and Aharon, 2010; Medina-Elizalde et al., 2017), we can estimate precipitation change from stalagmite $\delta^{18}O$ variability by shifting the annual precipitation cycle today by amounts that would yield the annual shifts in precipitation $\delta^{18}O$ that explain stalagmite $\delta^{18}O$ annual variability (Medina-Elizalde and Rohling, 2012). This method to produce quantitative precipitation estimates from stalagmite $\delta^{18}O$ was validated for the YP by comparisons with regional lacustrine sediment density and $\delta^{18}O$ records (Medina-Elizalde and Rohling, 2012). Since then, two other stalagmite $\delta^{18}O$ records have provided quantitative estimates of precipitation variability for the late Holocene and last glacial interval (Medina-Elizalde et al., 2016b, 2017).

The working hypothesis underlying this study is that stalagmite $\delta^{18}O$ records from the YP, at the locale of the study area, the Río Secreto cave system, provide quantifiable information of precipitation amount because there is a regional relationship between precipitation amount and precipitation $\delta^{18}O$ (i.e. amount effect), and stalagmites can represent equilibrium isotopic conditions with drip water (Medina-Elizalde et al., 2016a, 2016b, 2017). The latter is a necessary condition to produce quantitative precipitation estimates from stalagmite $\delta^{18}O$ records, but the actual values of equilibrium cannot be predicted theoretically and therefore are only approximated with empirical studies (Tremaine et al., 2011). This study reconstructs past precipitation variability from the oxygen isotopic composition ($\delta^{18}O$) of a stalagmite named Katún (after the Maya unit of time the K'tun equivalent to 7,200 days). The stalagmite Katún $\delta^{18}O$ record spans the interval between 198.6 and 322.7 thousand years (kyr) before present (BP). The Katún stalagmite specimen was collected from the Río Secreto Cave System, located in

Playa del Carmen; a cave that receives over 100,000 tourists per year and that has been the subject of an intense monitoring system over the last 5 years (Lases-Hernandez et al., 2018).

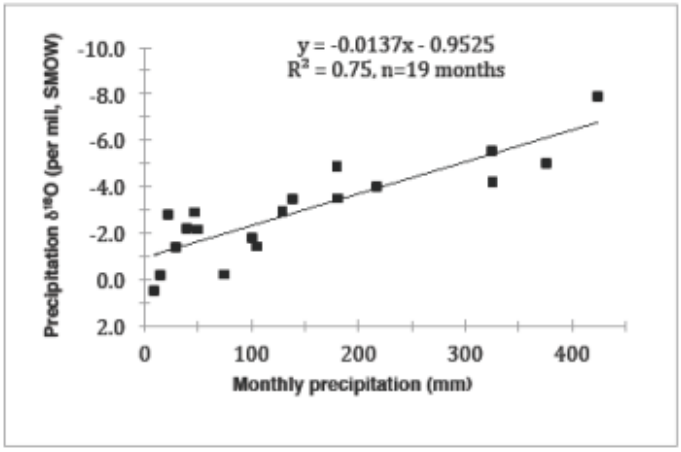

Figure 4) Precipitation $\delta^{18}O$ and precipitation amount measured monthly in Cancun and Playa del Carmen, Mexico between June 2012 and October 2014. The slope of this relationship is shown to represent the amount effect ($\delta P/\Delta P = -0.0137‰$ per mm ± 0.0031‰ per mm) in the YP (Medina-Elizalde et al., 2016b).

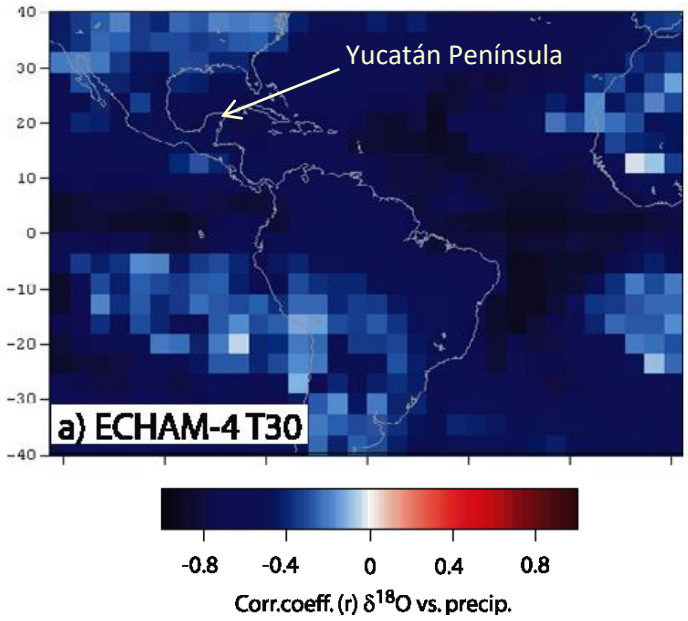

Figure 3) ECHAM-4 atmospheric general circulation model with incorporated stable isotopic tracers showing interannual variability in the YP (Vuille et al., 2003).

1.2. Background information

Tropical speleothem $\delta^{18}O$ measurements are used to reconstruct regional hydrological variability from decadal to glacial-interglacial timescales in tropical regions (Burns et al., 2002;

Medina-Elizalde et al., 2016b; Medina-Elizalde and Rohling, 2012; Cheng et al., 2012). In particular, as mentioned previously, tropical rainfall $\delta^{18}O$ variability is inversely correlated with precipitation amount (i.e. the amount effect) in the YP and Central America (Lachniet and Patterson, 2009; Medina-Elizalde et al., 2016a). The seasonal amount effect relationship between precipitation $\delta^{18}O$ and precipitation amount had not been directly measured in the YP until 2012 whereby a study by Medina-Elizalde et al. (2016b) began monitoring both rainfall $\delta^{18}O$ and rainfall amount in the city of Cancun, and in Río Secreto from the year 2014. Rainfall samples were collected and measured from June 2012 to October 2014 from individual precipitation events which were stacked in monthly samples (n = 19 months). Monthly sample $\delta^{18}O$ compositions were then determined to characterize the amount effect relationship (Fig. 3) (Medina-Elizalde et al., 2016b). The study by Medina-Elizalde et al., (2016b) confirms the existence of an amount effect on seasonal timescales in the YP with an amount effect slope of $\delta P/\Delta P = -0.0137 \pm 0.0031‰$, whereby δP corresponds to the change in the $\delta^{18}O$ composition of rainfall associated with a change in the amount of precipitation (ΔP) (Medina-Elizalde et al., 2016b). The amount effect recorded in the YP is statistically similar to that recorded in Veracruz, Mexico, and San Salvador, El Salvador (Lachniet and Patterson, 2009; Medina-Elizalde et al., 2016b). Furthermore, the oxygen isotopic composition of rainfall in the YP is not only controlled by the amount effect on seasonal timescales but on interannual timescales as well, as determined by the ECHAM-4 atmospheric general circulation model (GCM; Fig. 4) by Vuille et al. (2003).

1.3. Problems and hypotheses

1.3.1. Millennial timescales

During the last ice age (21 kyr BP), climate in the North Atlantic oscillated on millennial timescales in cycles referred to as Dansgaard-Oeschger (D-O) events which represent oscillations from cold (stadial) to warm (interstadial) episodes (Dansgaard et al., 1984; Oeschger et al., 1984). D-O events were first described in Greenland ice cores but have since been identified in speleothems, terrestrial lakes, and marine sediments from lower latitude regions in the North Atlantic, South America, Pacific and Indian Oceans (Hendy and Kennett, 2000; Wang et al., 2001; Hodell et al., 2008b; Deplazes et al., 2013; Peterson et al., 2000; Kanner et al., 2012) leading to increasing evidence that D-O events were closely linked to hydrological responses in tropical and subtropical regions, likely associated with the latitudinal position of the ITCZ. The prevailing hypothesis to explain precipitation variability on millennial-scale climate cycles invokes changes in AMOC (Broecker and Denton, 1990). During the last glacial, ice sheets in the Northern Hemisphere supplied enough freshwater to the North Atlantic to lower surface ocean density and ultimately reduce AMOC (Clark, 2001). AMOC slowdown resulted in cooling of the North Atlantic due to decreased heat transport from low to high latitudes (Broecker and Denton, 1990; Krebs and Timmermann, 2007). Consequently, this phenomena created a thermal asymmetry across the equator which led to a southward displacement of the ITCZ in the Pacific and Atlantic, which in turn enhanced precipitation in South America and diminished precipitation in North America and northern South America (Deplazes, Lückge, Peterson L. C., et al., 2013; Otto-Bliesner and Brady, 2010; Lewis et al., 2010; Stouffer, Yin, et al., 2006). Furthermore, models suggest that India and the North Atlantic can experience extreme precipitation reductions (up to 80%) induced by AMOC slowdown (Otto-Bliesner and Brady, 2010). However, the magnitude and frequency of tropical hydrological variability in the

Caribbean region resulting from AMOC slowdown remains predominantly unconstrained due to the lack of extensive rainfall records and discrepancies among existing records.

Climate evolution on millennial time scales in the northern Caribbean region has been investigated by several paleoclimate studies, but these offer contradicting results and none of these records continuously cover glacial-interglacial hydroclimate conditions to investigate orbital forcing. Paleoclimate records from only two locations in the northern Caribbean, from Lake Petén Itza, Guatemala (Hodell et al., 2008a; Escobar et al., 2012; Correa-Metrio 2012) and Playa del Carmen, Mexico (Medina-Elizalde et al., 2017), are of sufficient length to investigate climate variability on millennial time scales. Two records from the same location, Lake Petén Itza, Guatemala, are the magnetic susceptibility and ostracod $\delta^{18}O$ records that span the last 45,000 kyr to cover the last glacial interval and Holocene (Fig. 5). The magnetic susceptibility record (Fig. 5a) reflects changes in sediment lithology with clay-rich horizons (high magnetic susceptibility) being associated with wet climate intervals and gypsum deposits(low magnetic susceptibility) associated with dry climate intervals (Hodell et al, 2008, Escobar et al., 2012). The $\delta^{18}O$ record (Fig. 5b) is a record of precipitation based on ostracod $\delta^{18}O$ (Escobar et al., 2012). These proxy records, however, are not consistent in terms of interpreted patterns of climate variability during the past 40 thousand years. For example, although the Lake Petén Itza magnetic susceptibility record suggests that the southern Caribbean was wetter during the last glacial maximum (24-19 ky BP) than the entire Holocene (Fig. 5a; Escobar et al., 2012). Ostracod $\delta^{18}O$ records from the same sedimentary archive suggest that the Holocene was the wettest interval of the last 40 kyrs (Fig. 5b; Escobar et al., 2012). Conversely, a stalagmite $\delta^{18}O$ record from the northeastern YP suggests that Caribbean climate was both wetter and drier than today during the last glacial, between 26 and 23 kyr BP (Fig. 6; Medina-Elizalde et al., 2017).

Under the assumption that the ITCZ was pushed southward during the last glacial time interval as modeling and paleoclimate studies suggest (Arbuszewski et al., 2013; Baker et al., 2001; Chiang et al., 2003; Deplazes et al., 2013; Peterson and Haug, 2006), a pattern suggesting that the northern Caribbean was wetter during the last glacial would be inconsistent with the hypothesized role of the ITCZ in controlling precipitation regimes in the Caribbean region

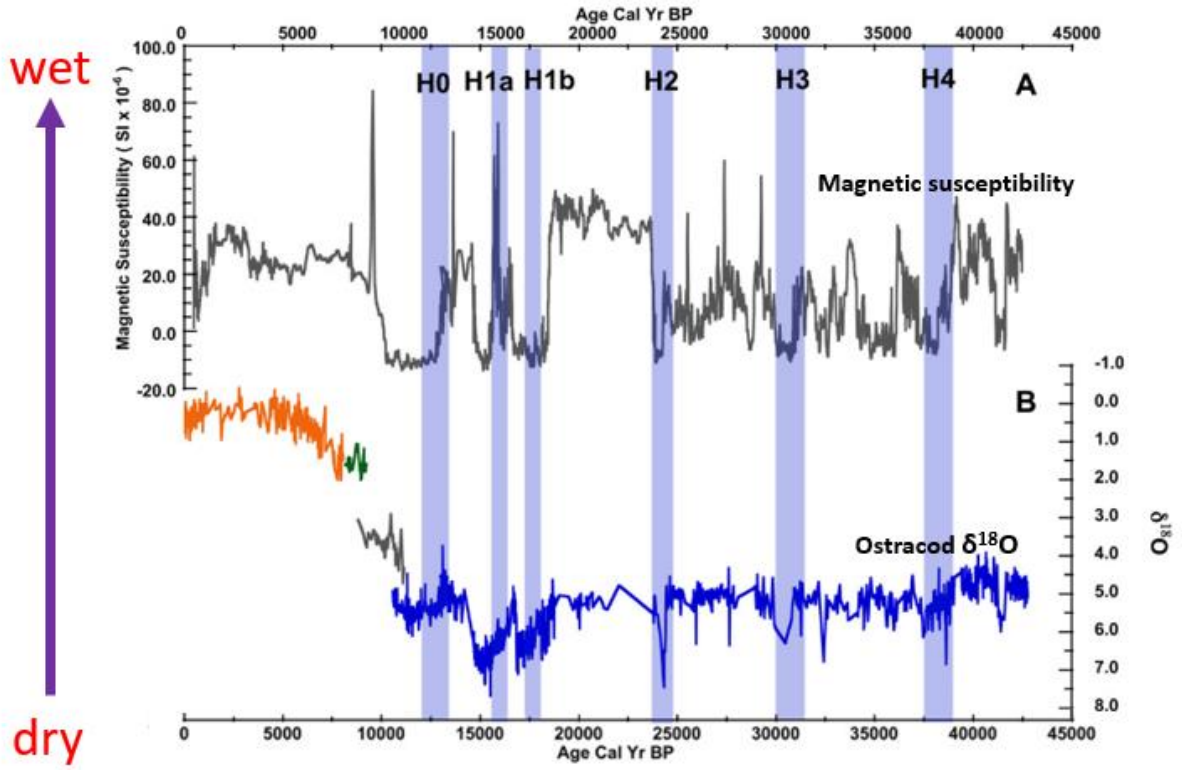

Figure 5) (A) Magnetic susceptibility record from site PI-6, Lake Petén Itza, Guatemala, LGM period shows wet conditions relative to dry Holocene conditions. (B) Oxygen isotope data for Lake Petén Itzá $\delta^{18}O$ data indicated by a blue line (Limnocythere opesta) are from PI-6. $\delta^{18}O$ data indicated by a grey line (Limnocythere sp.) are from Lake Petén Itzá core 11A (Hillesheim et al., 2005). $\delta^{18}O$ data indicated by an orange line (Cytheridella ilosvayi) and a green line (Pseudocandona sp.) are from Lake Petén Itzá core 6-VII-93 (Curtis et al., 1998). Adapted from Escobar et al., 2012.

(Fensterer et al., 2013; Haug et al., 2003; Hodell et al., 2008a). In addition to the differences among proxy-records from the same archive, the Lake Petén Itzá ostracod $\delta^{18}O$ records do not suggest climate patterns similar to paleoclimate records from other tropical locations. In particular, these records do not show millennial variability characteristic of the Greenland ice cores that is also observed in other low latitude records (Deplazes et al., 2013; Escobar et al., 2012; Kanner et al., 2012; Peterson and Haug, 2006). Pollen analyses from the same lake, furthermore, do suggest a potential link between tropical and high latitude climate on millennial time scales (Correa-Metrio et al., 2012; Hodell et al., 2008a). New low latitude paleoclimate records from independent terrestrial archives (e.g. stalagmites) would help evaluate high latitude forcing of tropical climate regimes on millennial time scales and clarify the source of discrepancies among available regional paleoclimate records. Particularly, new records could help answer the fundamental question whether the Caribbean was wetter or dryer during glacial relative to interglacial intervals.

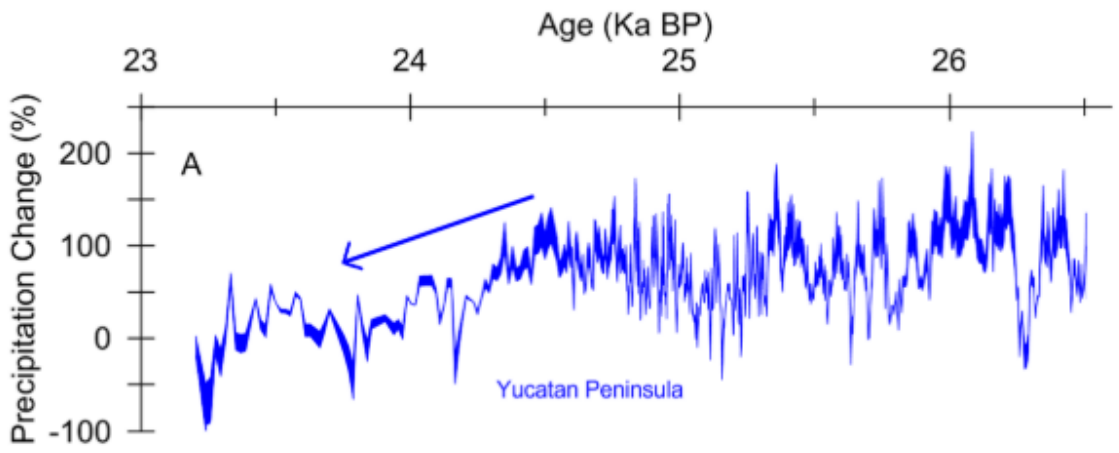

Figure 6) Precipitation amount record from the YP spanning the LGM indicating precipitation percent change relative to today (Medina-Elizalde et al., 2017).

1.3.2. Orbital timescales

Monsoonal records are of common interest in paleoclimate investigations because they are the dominant seasonal mode of climate variability in the tropics and the source of climate extremes affecting billions of people, particularly in Africa and Asia (Mohtadi et al., 2016). Monsoon systems are strongly influenced by large-scale meridional temperature gradients and the ITCZ position, which in turn are sensitive to forcing by different processes (Mohtadi et al., 2016). Paleo-monsoon records show seasonal-to-orbital-scale variability influenced by insolation forcing. Paleoclimate studies suggest that seasonal insolation variability driven by precession represents the main forcing of the South American, Southeast Asian, and West African monsoons (Cruz et al., 2005; Wang et al., 2001; Cheng et al., 2013a, 2016; Patricola and Cook, 2007). Additionally, stalagmite $\delta^{18}O$ records of precipitation from Borneo also suggests that precession is the dominant forcing factor on orbital timescales (Carolin et al., 2016; Meckler et

al., 2012). Currently available paleo-precipitation records from the Caribbean region are of insufficient duration to test the hypothesis that precession also drives precipitation variability in this region: ***Is precipitation variability in the Caribbean controlled by precession on orbital timescales?***

The only record from the Caribbean that covers a full glacial-interglacial interval is the Cariaco Basin (CB) sediment reflectance record that span the last 100 kyr (Deplazes et al., 2013). This record is a high-resolution record (0.2 years) of sediment color which measures terrigenous versus biogenic content. The CB sediment reflectance record shows pronounced D-O type variability and suggests that hydroclimate variability in the Caribbean is dominated by millennial scale variability (Deplazes et al., 2013). Specifically, this study finds that the ITCZ was permanently displaced south during glacial states which reflected a decrease in precipitation during the Indian summer monsoon both driven by variations in mean Northern Hemisphere temperature (Deplazes et al., 2013). The CB record does not show dominant orbital scale variability and most closely compares with the NGRIP ice core record which primarily reflects millennial scale variability.

Climate model studies predict an increase in total monsoon rainfall and monsoon expansion during the twenty-first century in response to rising atmospheric greenhouse gas (GHG) forcing (IPCC 2014). Climate model results from the TraCE-21k transient simulations of the last glacial termination, furthermore, suggest that GHG forcing, specifically CO_2, can play an important role in controlling rainfall variability and, in particular, in the intensity of the north African monsoon, also in the tropical Atlantic (Otto-bliesner et al., 2014; Mohtadi et al., 2016). Conversely, Mohtadi et al., (2016) points out that the lack of glacial–interglacial variability in paleo-rainfall records from deep tropical monsoon systems beyond the last glacial termination

indicates that GHG forcing does not play a dominant role. ***Is Caribbean hydroclimate sensitive to GHG forcing on glacial-interglacial timescales as suggested by climate model simulations for the African monsoon and future climate (Otto-bliesner et al., 2014)?***

1.4 Objectives

This study exploits the unique opportunity provided by a new stalagmite $\delta^{18}O$ record to reconstruct precipitation variability spanning a full glacial interglacial cycle in order to investigate millennial and orbital timescale climate variability preceding the last glacial interval. Particularly, this study seeks answers to the following relevant questions:

i. What is the amplitude and frequency of hydroclimate variability in the Caribbean region between 320 and 198 kyr BP?
ii. Was precipitation variability in the Caribbean controlled by precession on orbital timescales?
iii. Does millennial scale hydroclimate variability in the Caribbean region extend beyond the last glacial interval? If so, what are the dominant periods of variability and are they temporally continuous over glacial-interglacial time intervals?
iv. Was Caribbean hydroclimate sensitive to greenhouse gas (GHG) forcing on glacial-interglacial timescales as suggested by climate model simulations for the African monsoon and future climate (Otto-Bliesner et al., 2014)?

2. Methods

2.1. Speleothem collection and location

The 68-cm long stalagmite Katún specimen was retrieved from an isolated cave chamber in the Río Secreto, Natural Reserve; a semi-inundated cave system located in Playa del Carmen, in the northeast of the YP (20° 35.244'N; 87° 8.042'W) (Figs. 7, 8). The stalagmite was collected in May 2013 by Dr. Martin Medina-Elizalde. Katún was upright but no longer actively growing and was harvested near its base. It was shipped to the University of Massachusetts Amherst where it was cut lengthwise and polished. The stalagmite presents visually distinctive laminations, which do not represent annual depositions.

2.2. Speleothem chronology

The speleothem Katún time scale was determined from 9 absolute U-Th dates (Table 1), following established methods (Cheng et al., 2013b; Shen et al., 2003, 2012). Calcite powders weighing from 60 to 150 mg were used for Uranium and Thorium chemistry (Shen et al., 2003). U-Th isotopic measurements were conducted on a multi-collector inductively coupled plasma mass spectrometer (MC-ICP-MS), Thermo Fisher Neptune, at the High-Precision Mass Spectrometry and Environment Change Laboratory (HISPEC), Department of Geosciences, National Taiwan University and the David McGee Laboratory in the Massachusetts Institute of Technology (Shen et al., 2012). A triple-spike, ^{229}Th-^{233}U-^{236}U, isotope dilution method was employed to correct for mass bias and determine all uranium and thorium isotopic and concentration values in an off-line data reduction process developed by Shen et al. (2002). Dating is based on the U-Th disequilibrium technique which is based on the decay of the parent isotope ^{238}U into its daughter ^{230}Th. All errors of isotopic data and dates given (Table 1) are two

Figure 7) The stalagmite Katún used for $\delta^{18}O$ analysis in this study. Specimen is 68-cm long. Microsamples were taken along Katún's main growth axis and can be seen as a fine line running down the left side of Katún. U-Th dates (in years BP) and errors are shown to the right with a 100 ky hiatus in the younger portion of the specimen.

Figure 8) Map of the Yucatan Peninsula. Red circle marks location of Río Secreto Natural Reserve located near the eastern coast of the peninsula.

standard deviations. Errors range from 1422 years to 5978 years with errors increasing with depth. While these errors are large, they are not unusual in stalagmite specimens of this age and are associated with the characteristically low initial amount of uranium in samples from the YP. The stalagmite Katún's age model was created based on 2000 Monte Carlo simulations using the COPRA toolbox for MATLAB software (Fig. 9; Breitenbach et al., 2012). U-Th dates suggest that Katún grew continuously for 124,088 years from 322,775 years BP to 198,687 years BP and, after a long-hiatus, from 97,177 to 87,923 years BP. This study focuses on the oldest portion of the Katún stalagmite (designated as 68-15.5 cm from the top).

2.3. Cave monitoring

A study of drip water data conducted over three consecutive years revealed that drip water data at seventeen different drip sites within Río Secreto integrate the annual amount-

weighted $\delta^{18}O$ composition of rainfall (Lases-Hernandez et al., 2018). Instrumental precipitation and isotope data suggests that the $\delta^{18}O$ composition of precipitation in the Caribbean region and the YP in particular, reflects precipitation amount (i.e. the amount effect) from seasonal to interannual time scales, as mentioned previously (Vuille et al., 2003; Lachniet, 2009; Medina-Elizalde et al., 2016a, 2016b; Rozanski et al., 1993). Stalagmite $\delta^{18}O$ records from Río Secreto are thus expected to reflect the local amount effect ($\delta P/\Delta P$ =-0.0106‰/mm and -0.0168‰/mm; Medina-Elizalde et al., 2016b, 2017) and provide a faithful record of local to regional precipitation variability. A regional representation is supported by spatio-temporal correlation analysis (Fig. 1) that indicate that interannual precipitation variability in the broad Caribbean region is significantly correlated with precipitation in the YP (Medina-Elizalde et al., 2017).

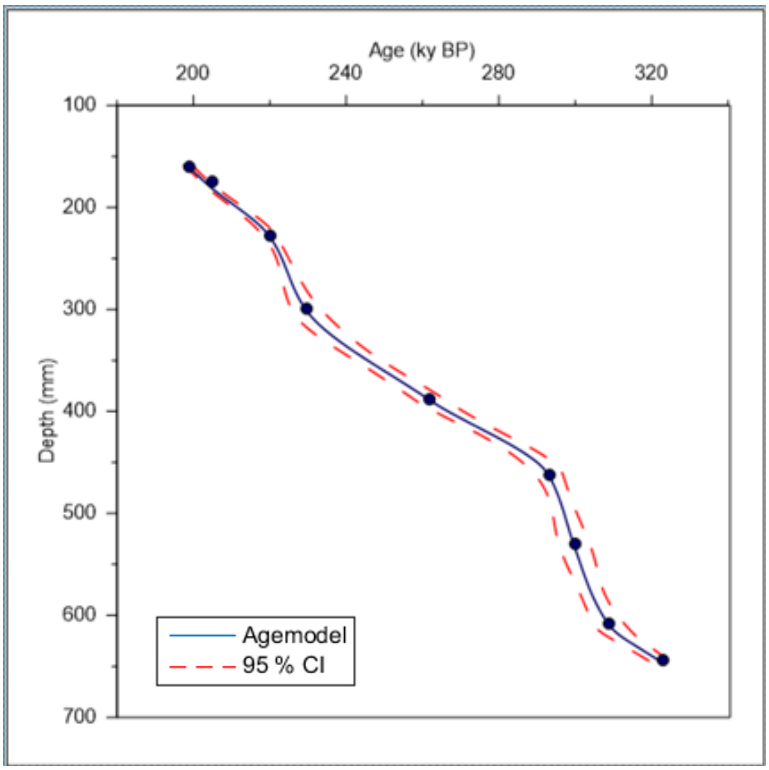

Figure 9) Katún's mean age model of the oldest section created by running over 2000 Monte Carlo simulations in the COPRA toolbox for Matlab software giving a 95% confidence interval (Breitenbach et al., 2012).

Relative humidity of Río Secreto was monitored over the course of two full years, from June 2014 to June 2016 (n = 5000 measurements using HOBO instruments; Medina-Elizalde et al., 2016b; Lases-Hernandez et al., 2018). A relative humidity of 100% was recorded throughout the study. These results were expected because the cave floor is currently below the water table and thus provides a constant moisture source that is particularly retained in cave chambers. The conditions were likely different during the last glacial when sea level, and thus the water table in the cave, were much lower than today. However, relative cave humidity during the last glacial may have remained close to 100% due to lower evaporation resulting from global cooling. Additional studies from caves without standing water in the northwest most arid region of the YP record relative humidity at or near saturation levels (Medina-Elizalde et al., 2010). These studies also monitored cave air temperatures from Río Secreto for 1.5 years from June 2015 to October 2016 (n > 1787 measurements using HOBO instruments; Medina-Elizalde et al., 2016b; Lases-Hernandez et al., 2018). Measured cave air temperature in the cave was 23 ± 1°C thus reflecting 3°C colder mean temperature than the annual mean air temperature in Playa del Carmen of 26°C (CONAGUA, 2012).

2.4. Stalagmite $\delta^{18}O$ composition

The stalagmite Katún oxygen isotopic composition was determined from 660 calcite powder microsamples drilled along its main growth axis using a Sherline 2010 vertical mill fitted with a drill bit 1.0 mm in diameter. The sampling resolution was 0.5 mm and 1 mm, yielding an average temporal resolution of 181 years. The oxygen isotopic composition of calcite powders was analyzed with a Thermo Scientific Delta V Plus Isotope Ratio Mass Spectrometer. The corresponding calcite oxygen isotope ratios are recorded in delta notation per mil ($\delta^{18}O$) where $\delta^{18}O$ values are the per mil difference between the sample and the IAEA standard in delta

notation where $\delta^{18}O = (R_{sample}/R_{standard} - 1) * 1000$, and R is the ratio of the minor to the major isotope. A Hendy test, used to assess whether isotopic equilibrium existed during the time of calcite deposition, was also performed along prominent laminations on the top section of Katún where five powder microsamples were drilled and analyzed to determine their stable isotope composition (Fig. 10). A Hendy test was not performed in the oldest section because visual laminations do not represent annual or higher resolution depositions, and therefore conventional sampling protocols would not yield samples taken across the exact same temporal frame and would not provide a robust test of isotopic equilibrium depositions *sensu* (Dorale and Liu, 2009; Hendy, 1971). We do not have direct evidence that the Katún $\delta^{18}O$ values reflect isotopic equilibrium conditions with drip water $\delta^{18}O$, because we cannot apply a Hendy test rigorously with conventional sampling techniques. However, we find indirect evidence that supports that the stalagmite $\delta^{18}O$ values reflect isotopic equilibrium conditions or near equilibrium, specifically: (i) comparisons between the Katún $\delta^{18}O$ values associated with interglacial conditions are similar to Holocene $\delta^{18}O$ values from two other stalagmite $\delta^{18}O$ records that do represent near equilibrium conditions; the Itzamna record from the Río Secreto cave (Medina-Elizalde et al., 2016b) and the Chaac record from cave Tzabnah in the northern YP (Medina-Elizalde et al., 2010); (ii) examination of relative humidity and temperatures of these caves (Río Secreto and Tzabnah) suggest consistent relative humidity of 100% and constant temperatures to within 2°C, associated with an annual temperature range exceeding 12°C, and; (iii) the last glacial Itzamna $\delta^{18}O$ record also from Río Secreto provides quantitative precipitation estimates which are consistent with climate model results (Otto-Bliesner and Brady, 2010) , thus suggesting consistent near equilibrium conditions on interglacial and glacial time scales within this cave system (Medina-Elizalde et al., 2017).

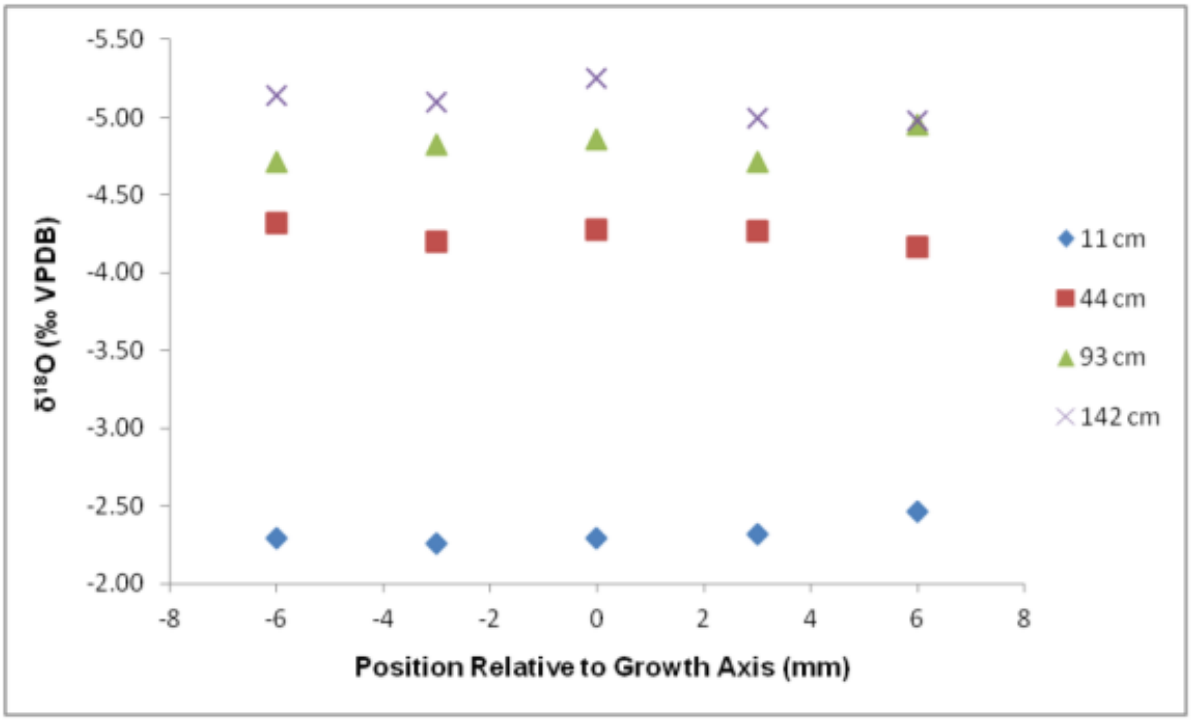

Figure 10) Hendy test on the Katún top section. Four laminations were sampled at the distances from the stalagmite top indicated in the legend. Lack of systematic variability in stalagmite $\delta^{18}O$ moving away from the growth axis indicates that the Katún top section grew under isotopic equilibrium conditions.

3. Results and Discussion

3.1. Speleothem oxygen isotope data and interpretation

This project focuses on the portion of Katún that grew over the time interval between 322 and 198 ky BP. We interpret the stalagmite $\delta^{18}O$ record to reflect variability in the local amount effect supported by instrumental observations and model data, and therefore the amount of precipitation as previously explained. On the other hand, because local precipitation in the YP is linked to the broader Caribbean region on interannual timescales, as supported by instrumental spatial correlation analyses of precipitation (Fig. 1), we assume that the stalagmite $\delta^{18}O$ variability also resembles broader scale hydroclimate change beyond the YP. The Katún stalagmite has an average $\delta^{18}O$ of -3.6‰, with a 2SD range from -2.1 to -5.1‰. This isotopic range is similar to that observed in the Itzamna stalagmite record spanning the late Holocene and last glacial maximum time intervals (Medina-Elizalde et al., Medina-Elizalde et al., 2017). The Katún record suggests that interglacials are wetter than glacials in the YP. Particularly, the Katún stalagmite indicates two distinctive time intervals of low amplitude variability and negative $\delta^{18}O$ values, interpreted to represent relatively wet conditions, between 320 ky BP – 280 ky BP and 245 ky BP – 198 ky BP. In contrast, the stalagmite indicates a distinctive time interval of positive $\delta^{18}O$ values, which indicate dry conditions at 275 ky BP – 250 ky BP. We find that Marine Isotope Stages (MIS) 7–9 from Lisiecki and Raymo's benthic foraminiferal $\delta^{18}O$ stack (hereafter, LR04; Lisiecki and Raymo, 2005) are readily identifiable within the Katún record. In particular, MIS 7c, 7e, and 9a represent the wettest, most negative $\delta^{18}O$ intervals, and glacial MIS 7d and 8a represent the driest, most positive $\delta^{18}O$ intervals Fig 11). A cross-correlation analysis between the Katún $\delta^{18}O$ record and LR04 support this visual comparison suggesting a positive correlation between the two time series with a Pearson correlation of 0.34 [0.17, 0.495]

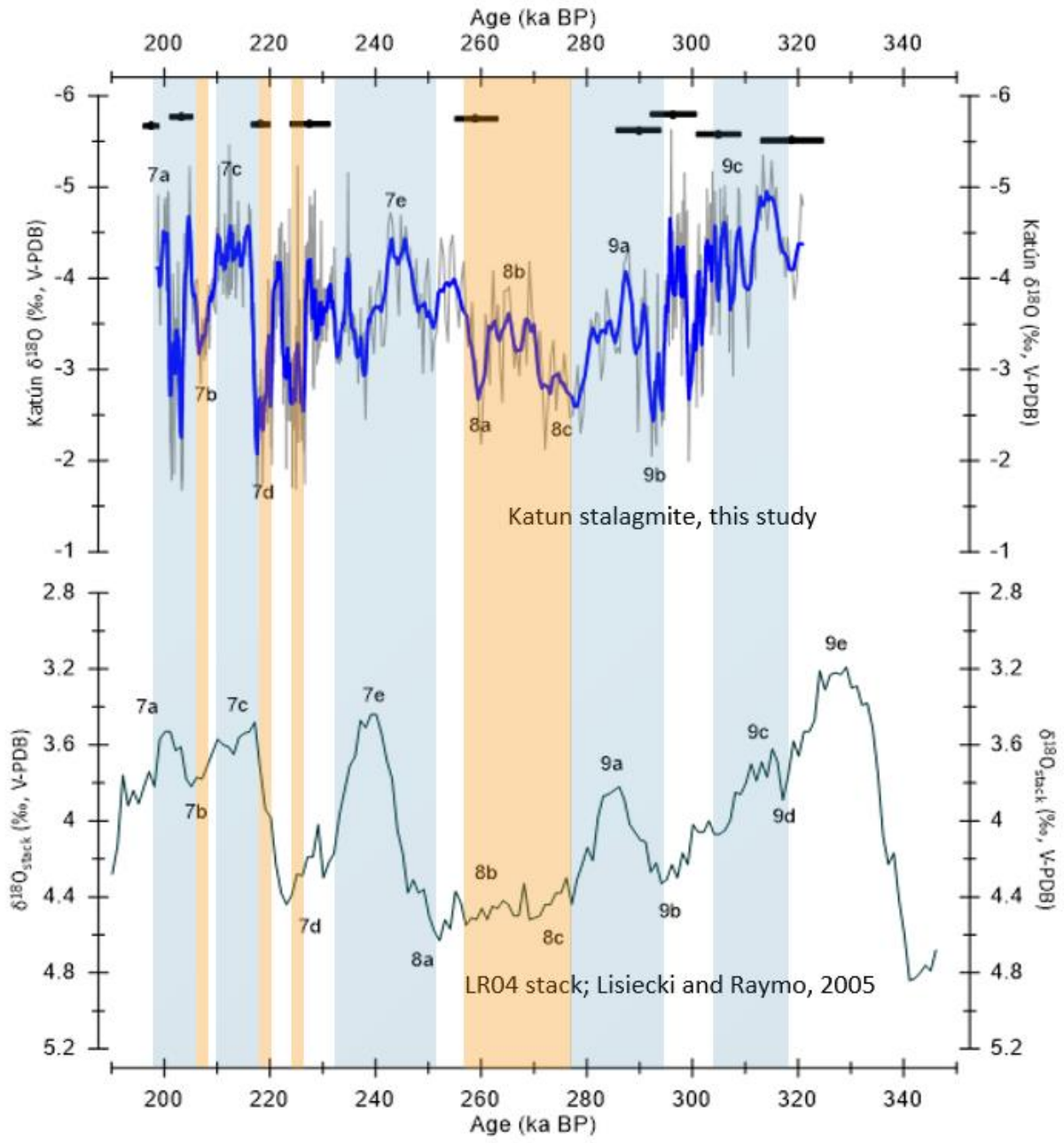

Figure 11) Top: Katún stalagmite $\delta^{18}O$ record. Blue line is $\delta^{18}O$ record with a 9-point running mean smoothing technique applied and gray line is the unsmoothed $\delta^{18}O$ record. Black error bars represent errors of the stalagmites 9 U-Th dates. Bottom: LR04 benthic foraminiferal $\delta^{18}O$ stack from Lisiecki and Raymo (2005). MIS 7a through 9c from the LR04 record are identifiable within the Katún record. Blue bars represent wet interglacial periods whereas orange bars represent dry glacial periods identified in both records.

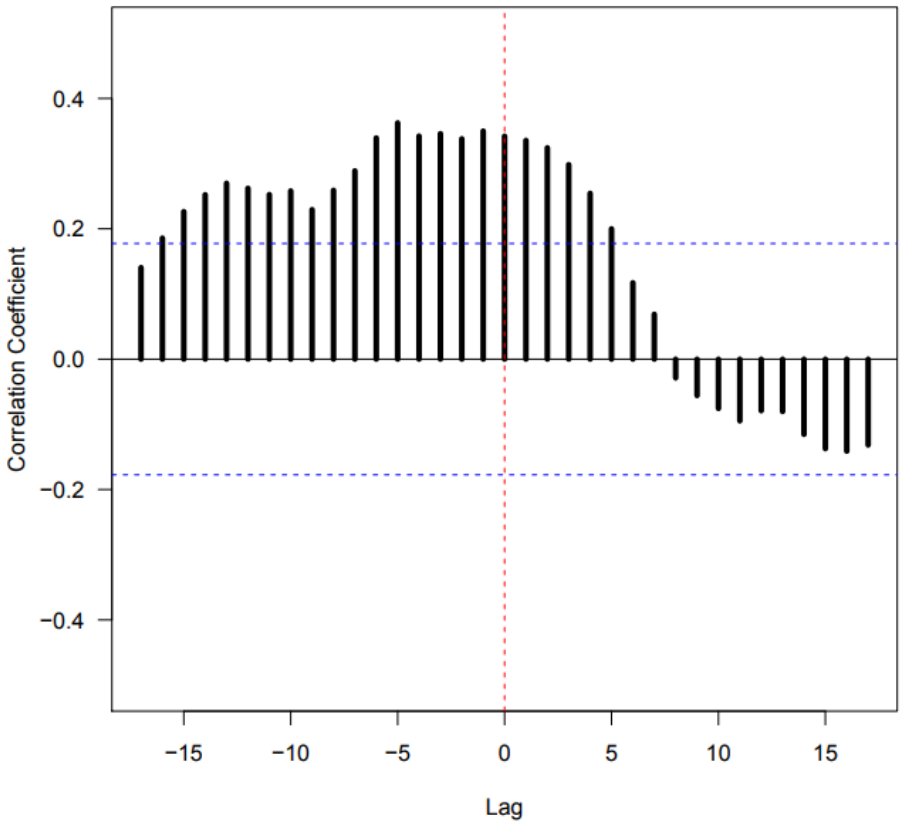

Figure 12) Cross correlation analysis between the Katún $\delta^{18}O$ record and LR04 interpolated at the LR04 time resolution; a positive correlation between the two records at lag-0 is found. The Pearson correlation is 0.34, with a 95% confidence interval [0.17, 0.49].

(Fig. 12). Another important observation is that the amplitude of $\delta^{18}O$ variability in the Katún record increases progressively during glacial inceptions; from modest amplitude variability (<0.2‰) associated with interglacial intervals MIS 7c and 9a to a much larger amplitude variability (>1‰) associated with MIS 8 glacial conditions (Fig. 13). The amplitude enhancement is mostly driven by progressively more positive $\delta^{18}O$ values including events in between with values as negative as those associated with interglacial conditions (Fig. 13). This pattern suggests that glacial intervals in the Caribbean experienced a higher propensity for intense precipitation reduction while wet intervals, similar to those found during the Holocene and previous interglacial intervals (MIS 7 and 9), continued occurring at times. This evidence is consistent with the Itzamna $\delta^{18}O$ record of the last glacial (Medina-Elizalde et al., 2017), which also suggests that precipitation during the last glacial maximum oscillated between values as

high as during the Holocene and were also much drier than this time interval. This result suggests that hydroclimate variability was enhanced during the transition from warm to cold conditions, when climate dynamical feedbacks associated with enhanced aerosols, ice sheet and sea ice extent, operating over glacial intervals, would have amplified multidecadal temperature and atmospheric moisture oscillations (Palaeosens, 2012).

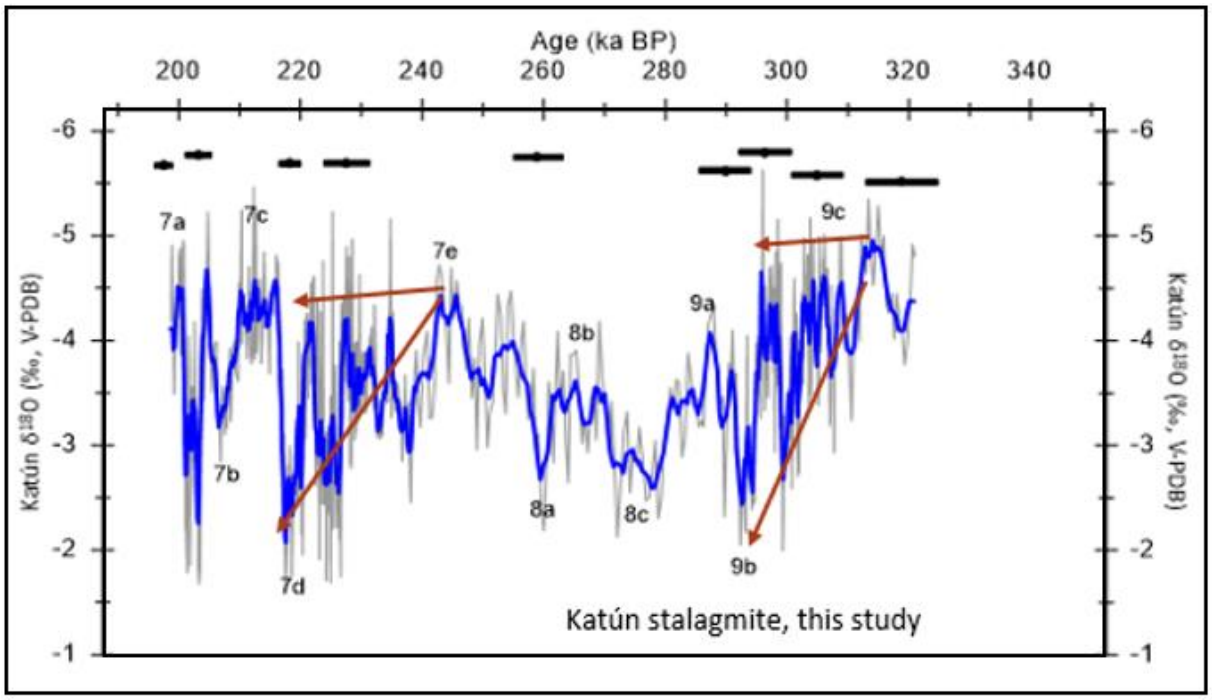

Figure 13) Katún stalagmite $\delta^{18}O$ record. Red arrows emphasize increasing amplitude variability where $\delta^{18}O$ values are becoming progressively more positive. MIS 9-7 and errors are indicated.

3.2. Millennial timescales

The Atlantic meridional overturning circulation (AMOC) is a major temperature and density dependent ocean current that delivers warm surface water to high northern latitudes and returns cold deep water to the tropics (Rahmstorf, 2002). Shifts in the intensity of AMOC have been hypothesized to greatly affect meridional heat transport with significant repercussions for global climate. Specifically, a high AMOC may cause the ITCZ to shift northward while

concurrently increasing the heat flux to the northern latitudes, thereby accounting for both increased precipitation on the YP and warmer surface temperatures in northern Greenland (Deplazes et al., 2013). Several potential controls on AMOC intensity have been proposed including orbital forcing and ocean temperature and salinity shifts (Rial and Yang, 2007; Bond et al., 2009). The Cariaco Basin sediment reflectance record from northern South America suggests that millennial scale oscillations, as those seen in Greenland, had a strong influence on Caribbean hydroclimate during the last glacial interval (last 100 kyr) (Deplazes et al., 2013). This record does not extend to cover the same time interval as the Katún stalagmite and reflects conditions over 1000 miles away from the YP. There is currently no other record reflecting terrestrial hydroclimate conditions over the same time interval covered by the Katún $\delta^{18}O$ record. In order to determine if there is any millennial scale variability present within the Katún record, we have performed a wavelet spectral power analysis (Lui et al., 2007; Torrence and Compo, 1998). Results of this analysis indicate significant millennial scale variability with periodicities between 4 and 8 kyrs (Fig. 14). The periodicities within the Katún record could be attributed to shifts in AMOC, which is the same mechanism that has been invoked to explain millennial scale variability in the Caribbean during the last glacial (Deplazes et al., 2013; Escobar et al., 2012Medina-Elizalde et al., 2017). Briefly, AMOC slowdown via freshwater forcing creates a thermal asymmetry across the equator that leads to a southward displacement of the ITCZ in the Atlantic and Pacific, which then enhances precipitation in South America and the opposite in North America (Chiang et al., 2008; Lewis et al., 2010; Otto-Bliesner and Brady, 2010; Stouffer, Broccoli, et al., 2006). Model results suggest, furthermore, that AMOC slowdown can induce intense precipitation reductions in the North Atlantic and India of up to 80% (Otto-Bliesner and Brady, 2010).

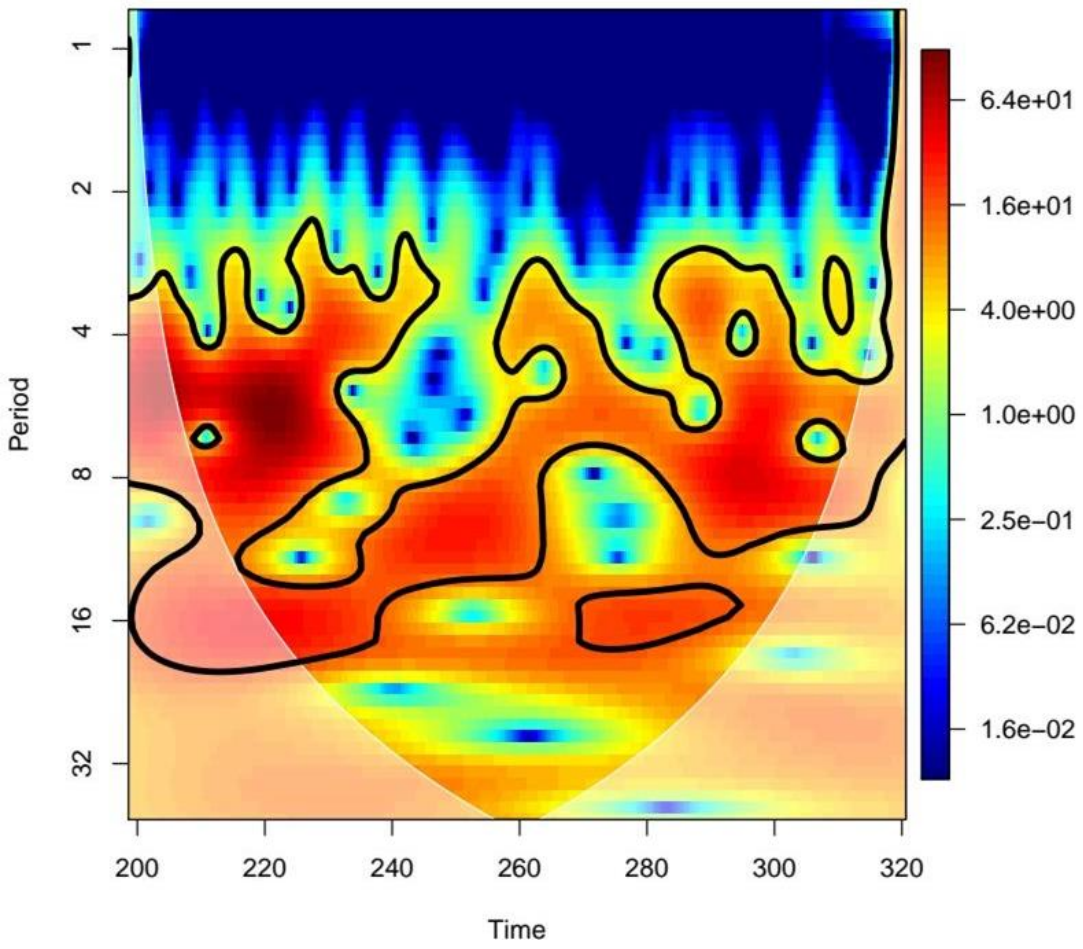

Figure 14) Wavelet spectral power analysis of the Katún $\delta^{18}O$ record that shows periodicities between 4 and 8 ky. The area outside the white lines indicates the cone of influence where the edge effects of the wavelet transform, and uncertainties become important (Lui et al., 2007; Torrence and Compo, 1998).

3.3. Orbital timescale

Monsoon records from Borneo (Wang et al., 2008) and China (Meckler et al., 2012) that span the last 600 ky BP suggest that precession is the dominant control of hydroclimate variability on glacial-interglacial timescales in those regions. It is important to note that these records primarily come from areas under monsoon-driven precipitation regimes in which

monsoon intensity and therefore precipitation amount varies in accordance with earth processional cycle. The precessional influence on monsoon intensity is thought to be linked to the influence of local seasonal insolation shifts on the atmospheric temperature gradient between the continent and ocean (Braconnot et al., 2007; Kutzbach and Guetter, 1986). As local insolation increases/decreases due to precession, the land is expected to warm/cool at a faster rate than the ocean, enhancing/suppressing the monsoonal circulation and thus the transfer of moisture from the ocean to the land surface (Kutzbach and Guetter, 1986). The YP is surrounded by the Gulf of Mexico on the West and North coasts, and by the Caribbean Sea on the East coast and its landmass is smaller by orders of magnitude than those associated with the Asian, African and South American monsoonal regions. Model studies, in fact, do not suggest a strong response of the North American Monsoon, including the YP region to orbital forcing, including climatic precession and obliquity (Mohtadi et al., 2016; Otto-bliesner et al., 2014). A visual comparison between the Katún stalagmite record (Fig. 15a) with the precession perimeter (Fig. 15b) does not suggest a connection. Furthermore, cross-correlation analysis between the stalagmite record and summer insolation changes between 18°N – 21°N, driven by climatic precession does not suggest a strong connection either (Fig. 16). Precession does not seem to provide a dominant control on Caribbean hydroclimate as observed during the last glacial in monsoon records from Borneo and China (Wang et al., 2008; Meckler et al., 2012).

We note that the sample resolution of the Katún record does not enable us to identify interannual precipitation variability that could be associated with El Niño-Southern Oscillation (ENSO). Studies with models and historical records suggest that YP precipitation regimes are modulated by ENSO, though the underlying mechanism remains still unclear (Karmalkar et al., 2011; Magaña et al., 2003; Mendoza et al., 2006). One possibility is that ENSO enters the

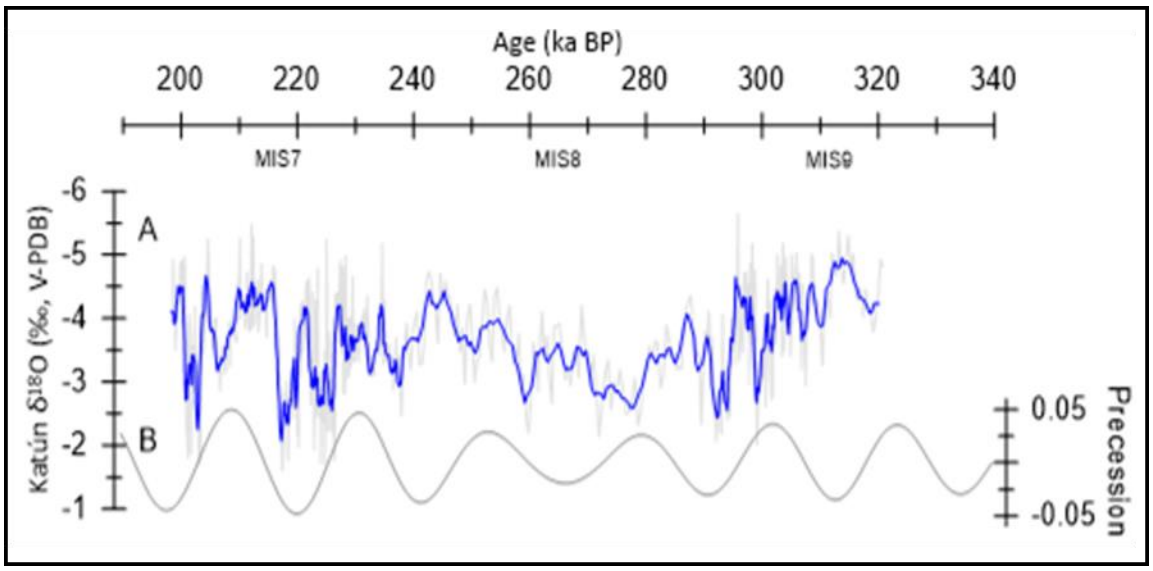

Figure 15) (A) Katún $\delta^{18}O$ record compared with (B) precession parameter between 18°N – 21°N. The precession parameter is defined as e*sin(ϖ) where ϖ is the longitude of the perihelion relative to the vernal point and e represents eccentricity.

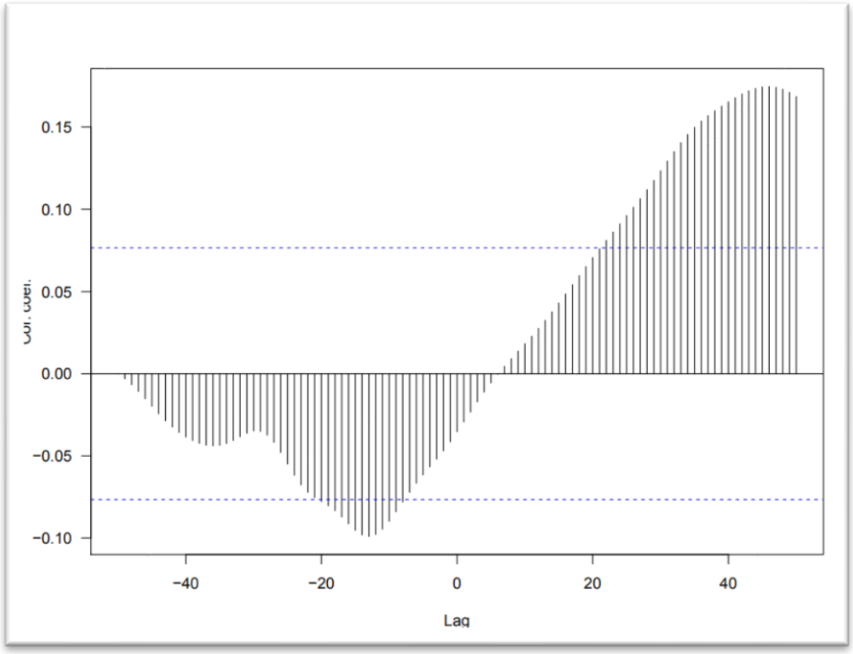

Figure 16) Cross-correlation analysis between the Katún $\delta^{18}O$ record and the precession parameter between 18°N – 21°N. 95% confidence interval is represented by dashed blue lines. We find that the lead-lag is significant within the chronological uncertainties of Katún but results in a low cross correlation coefficient (L 0.15).

paleoclimate record through modulating tropical Atlantic cyclogenesis. Atlantic hurricanes are suppressed when El Niño conditions in the Pacific induce upper altitude increased wind shear in the Atlantic, thus reducing rainfall fluxes over the YP by tropical cyclones (Goldenberg and Shapiro, 1996; Gray, 1984).

3.4. Katún vs. tropical SSTs and CO_2

Atmospheric CO_2 likely played a dominant role in controlling tropical sea surface temperature variability on orbital timescales as suggested by a number of paleoclimate studies (Shackleton, 2000; Medina-Elizalde and Lea, 2005; Herbert et al., 2010; Rohling et al., 2012; Palaeosens, 2012). Sea surface temperature, on the other hand, is recognized to influence hydroclimate variability in the Atlantic, including the Caribbean region. Instrumental, paleoclimate and modeling data support a link between multidecadal temperature oscillations in the North Atlantic, generally referred to the Atlantic Multidecadal Oscillation (AMO), and hydroclimate variability over large parts of the North Atlantic (Gray et al., 2004; Knight et al., 2006). Particularly for the Gulf of Mexico and Caribbean regions, model simulations and analyses of instrumental data show significant precipitation increases during the positive phase of AMO (warm) and vice versa during the negative phase (cold) (Alexander et al., 2014; Knight et al., 2006). Large-scale hydrological responses to AMO have been associated with variations in the SST gradient between the north and south Atlantic (Folland et al., 2002; Moura and Shukla, 1981) shifts in the mean Intertropical convergence zone (ITCZ; Knight et al., 2006) and changes in Atlantic tropical cyclogenesis (Goldenberg et al., 2001; Knight et al., 2006).

In order to determine if Caribbean hydroclimate is sensitive to forcing by atmospheric CO_2, we employ cross-correlation analyses between the Katún $\delta^{18}O$ record and the EPICA Dome C ice core record of atmospheric pCO_2 from Antarctica (Lüthi et al., 2004). I first examine this

comparison including the full record length, 198-322 ky BP. Visual inspection suggests a significant correlation between these two time series during interglacial intervals; therefore, I produced two zoomed-in comparisons of the records during these times. Cross-correlation analyses suggest that there is a significant correlation between these two records (Fig. 17; Pearson correlation r=-0.45 [CI 95% p= -0.57, -0.3]). That is, lower Katún $\delta^{18}O$ values, reflecting more precipitation, occur in association with high atmospheric CO_2 levels and vice versa in association with low atmospheric CO_2. I performed cross-correlation over the two selected shorter time intervals, 198-245 ky BP and 275-320 ky BP, that include transitions from high levels of atmospheric CO_2 associated with interglacial conditions to low CO_2 levels associated with glacial conditions (Fig. 18). Cross-correlation results suggest that the records are synchronous with a significant correlation (CI 95%) at lag zero equaling r=-0.53 and r=-0.84, for the 198-245 ky BP and 275-320 ky BP time intervals, respectively (Fig. 19). This statistical comparison supports the potential role of greenhouse gases (GHGs), specifically atmospheric CO_2, in driving hydroclimate variability in the Caribbean region.

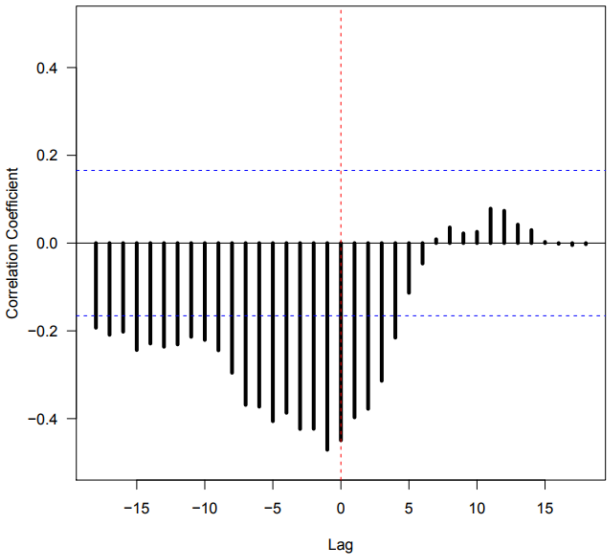

Figure 17) Cross correlation between the Katún $\delta^{18}O$ record and EPICA Dome C ice core record of pCO_2 by Lüthi et al. (2004), interpolated at 800 years with dashed blue lines representing the 95% confidence interval. There is a negative Pearson correlation of -0.45 [-0.57, -0.31] between the two records.

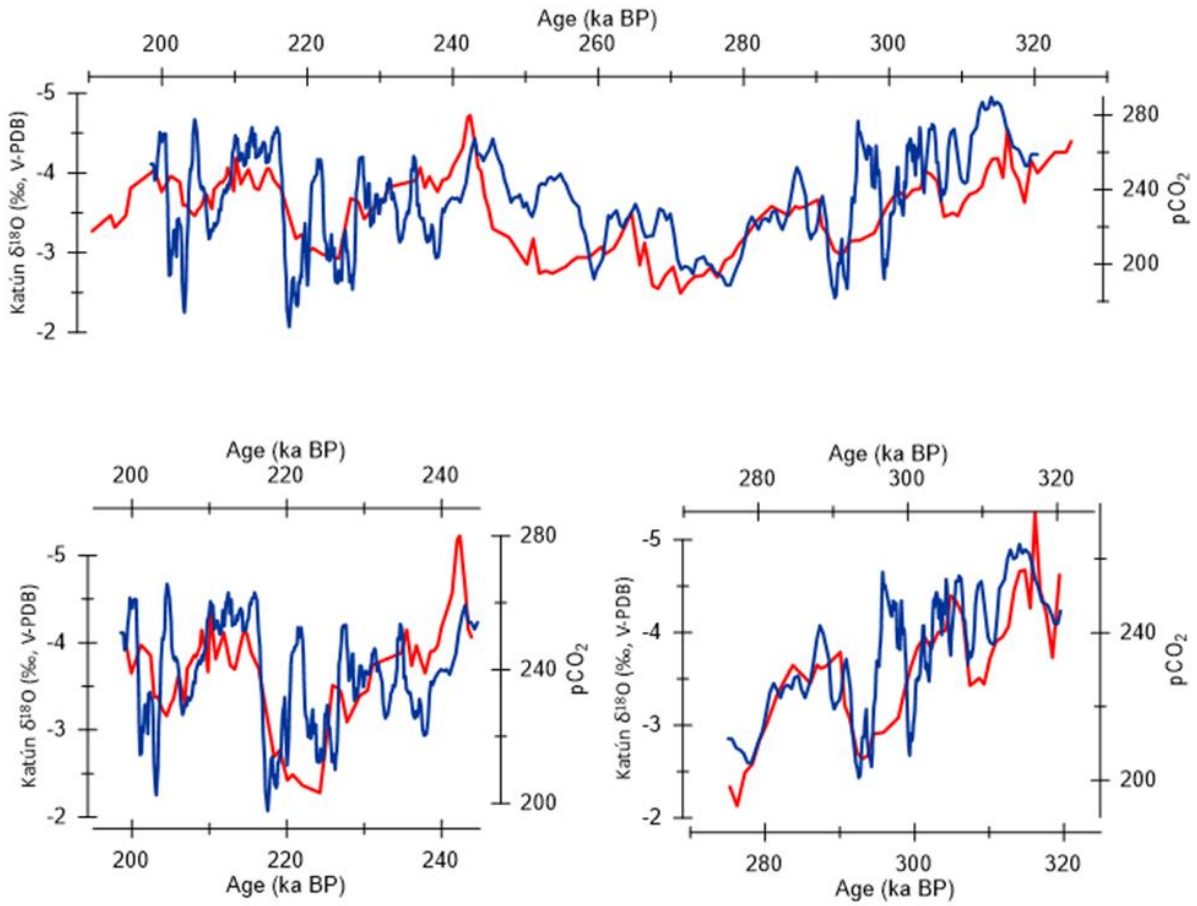

Figure 18) Comparison between the Katún $\delta^{18}O$ record (blue) and EPICA Dome C ice core record of pCO_2 (red) by Lüthi et al. (2004). Complete record reflects a negative Pearson correlation of – 0.53. Bottom left blow-up of interglacial time interval 198-245 ky BP and bottom right blow-up is of interglacial time interval 275-320 ky BP. Pearson correlation coefficients are -0.53 and -0.84 respectively, within the 95% confidence interval.

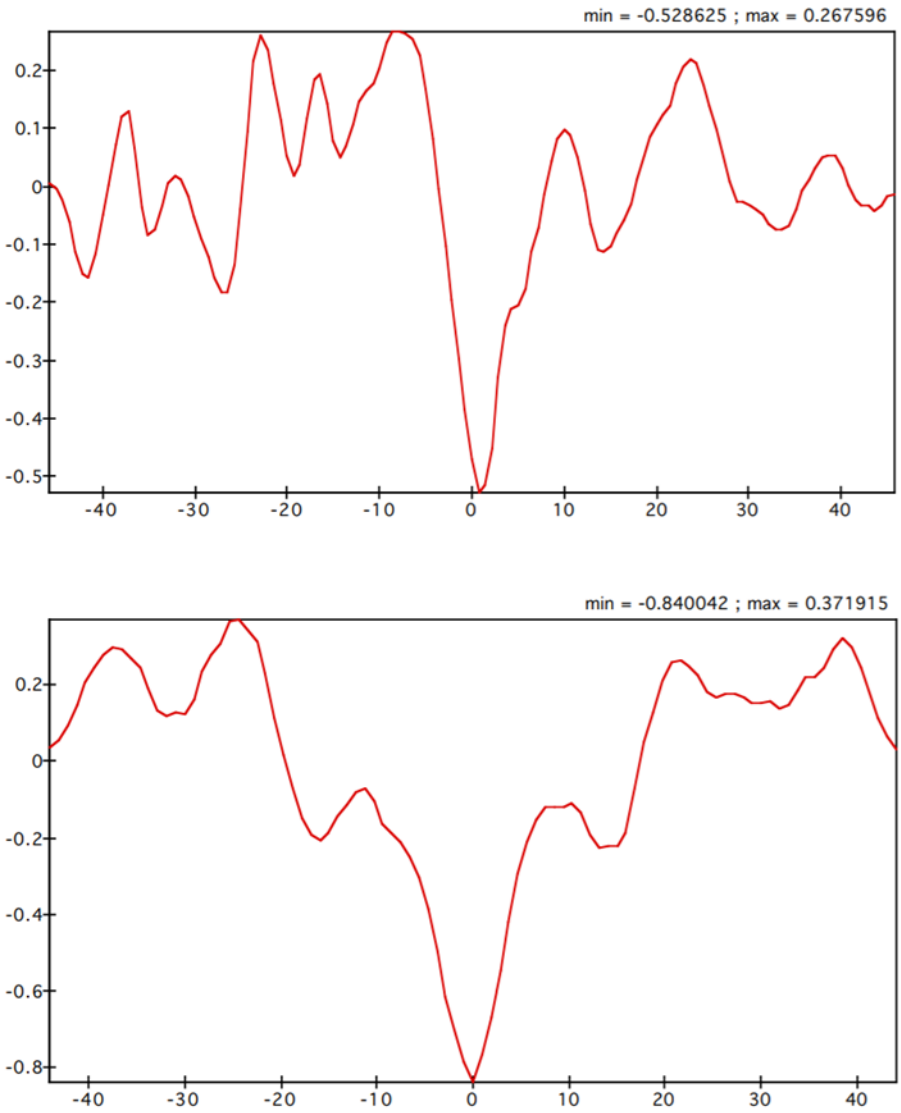

Figure 19) Cross correlation analysis between the Katún $\delta^{18}O$ record and EPICA Dome C ice core record of pCO_2 by Lüthi et al. (2004) for the time intervals of 198-245 ky BP (top) and 275-320 ky BP (bottom) interpolated at the pCO_2 time resolution with Analyseries software.

If CO_2 played a role in driving Caribbean hydroclimate, by which mechanism does the atmospheric CO_2 signal enter the hydroclimate record? Surface temperatures are a pronounced driver of hydroclimate change in the Atlantic and Caribbean region in the present, as presented previously. During glacial conditions lower surface temperatures, particularly tropical

temperatures, would be associated with lower atmospheric moisture content, a southern displacement of the ITCZ and its belt of convective activity, and ultimately decreased precipitation in the Caribbean as suggested by theoretical, modeling, and paleoclimate evidence (Held and Soden, 2006; Otto-Bliesner et al., 2014; Gray et al., 2004; Knight et al., 2006; Fensterer et al., 2001; Deplazes et al., 2013; Mohtadi at al., 2016).

To examine the relationship between the Katún record and surface temperature, we compare the stalagmite record with the tropical sea surface temperature stack by Herbert et al. (2010) which includes records from Ocean Drilling Program (ODP) core sites ODP662, ODP722, ODP846, IODP1146 located in the tropical Atlantic, Arabian Sea, East Pacific, and South China Sea, respectively, with a time resolution of about 3 kyrs (Fig. 20). Visual inspection of these records suggests that Katún $\delta^{18}O$ values decrease in association with an increase in

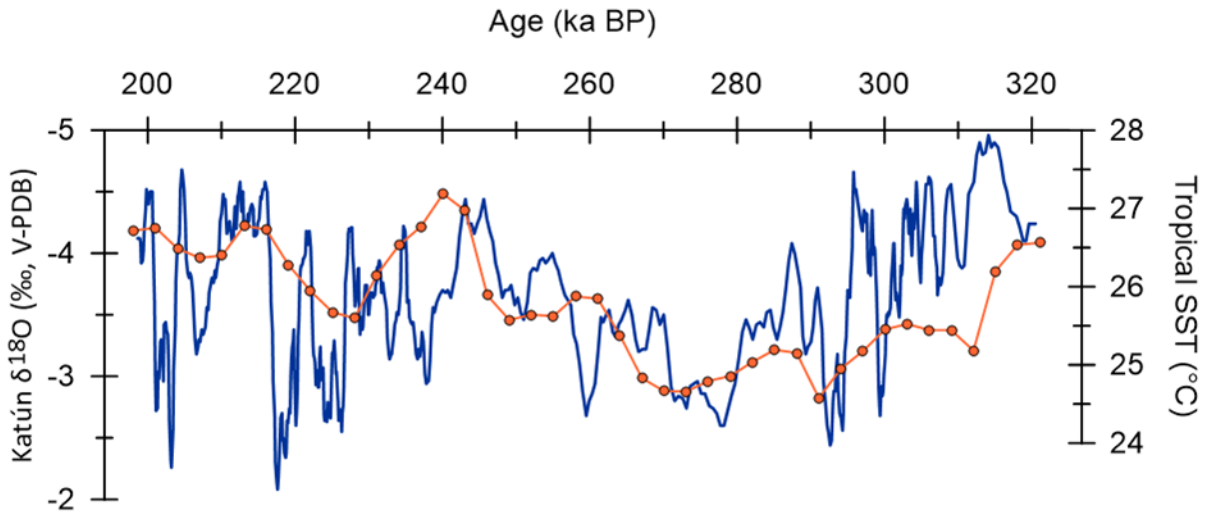

Figure 20) Comparison between the Katún $\delta^{18}O$ record (blue) the tropical sea surface temperature stack (orange) by Herbert et al., (2010). The SST stack has a time resolution of approximately 3 kyrs; orange dots represent data points.

tropical SSTs and the cross-correlation is also statistically significant with an r value of up to -0.7 (Fig. 21; Pearson correlation, r= - 0.5038062 [-0.704717, -0.228094]). This analysis suggests that precipitation in the YP and likely the Caribbean region was favored during times of high tropical Atlantic SSTs and atmospheric CO_2. We, therefore, suggest that atmospheric CO_2 by controlling tropical SST variability ultimately drove Caribbean hydroclimate variability between MIS 9 and 7. This connection is visually illustrated in a comparison between the Katún $\delta^{18}O$, tropical SSTs, and atmospheric pCO_2 records (Fig. 22). Higher CO_2 concentrations correlate with higher SSTs which results in warmer, wetter hydroclimate conditions in the Caribbean. In contrast, lower atmospheric CO_2 concentrations induce lower tropical SSTs which results in cooler, dryer Caribbean hydroclimate conditions. Lower ocean SSTs would reflect lower atmospheric temperatures, lower atmospheric moisture content and a southern displacement of the ITCZ and its belt of convective activity, ultimately lowering precipitation in the Caribbean and vice versa.

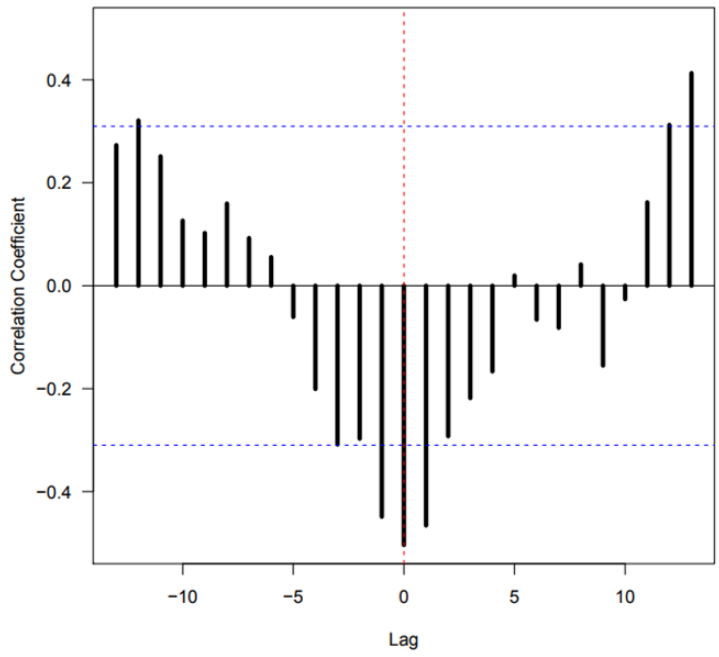

Figure 21) Cross correlation analysis between the Katún $\delta^{18}O$ record the tropical sea surface temperature stack by Herbert et al., (2010) interpolated to SST stack time resolution. Pearson correlation, r = -0.5038062 [-0.704717, -0.228094].

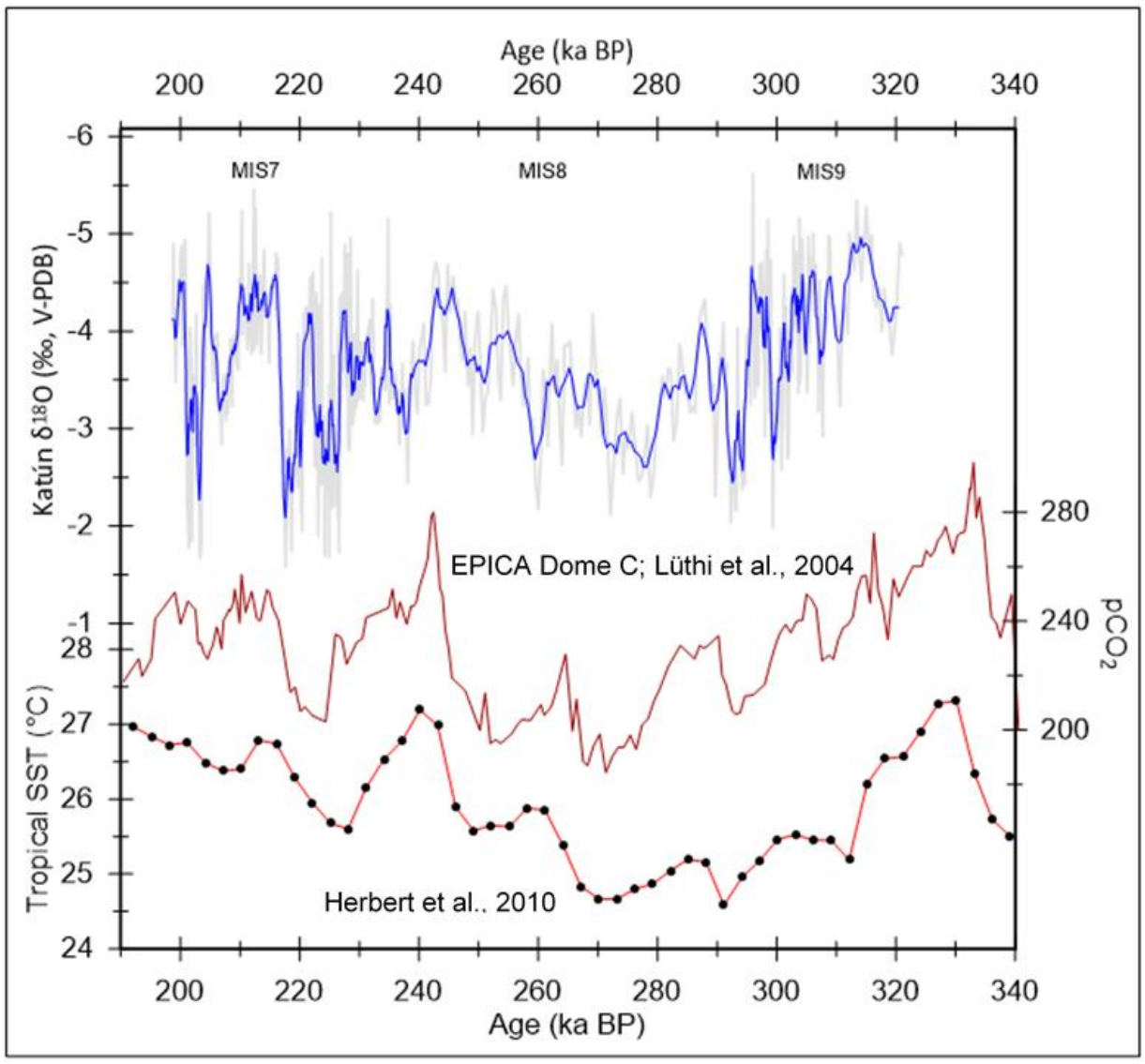

Figure 22) Comparison between the Katún $\delta^{18}O$ record (blue), EPICA Dome C ice core record of pCO_2 (red) by Lüthi et al. (2004), and the tropical sea surface temperature stack (orange) by Herbert et al. (2010). MIS 7-9 are indicated at the top, identified from the LR04 stack (Lisiecki and Raymo, 2004).

3.5. Disentangling the temperature component of Katún $\delta^{18}O$

One question that arises from the aforementioned statistically significant correlation between tropical SSTs and atmospheric CO_2 variability is whether the Katún $\delta^{18}O$ variability is controlled to some extent by cave temperature variability, via its effect on the thermodynamic

equilibrium between the isotopic composition of calcite and drip water. Tropical SST variability on glacial-interglacial time scales is expected to reflect thermal equilibrium conditions with the atmosphere (Palaeosens, 2012). Cave temperature variability, in turn, would be expected to reflect equilibrium with air temperature variability. We note today that the annual temperature in Río Secreto reflects the annual air temperature and therefore it is expected to vary on glacial-interglacial timescales when Caribbean temperatures oscillated with a range of about three degrees Celsius. We do not consider a significant continental effect on air surface temperatures in Playa del Carmen because of its closeness to the Caribbean, which is the main source of moisture and experiences the prevailing trade winds from the Atlantic. In order to evaluate the influence of cave temperature variability on Katún stalagmite $\delta^{18}O$ variability we extract the temperature component in this record using the SST compilation by Herbert et al., (2010). In order to extract the temperature component from the stalagmite $\delta^{18}O$ record we use the temperature isotopic sensitivity of -0.17‰/°C from Tremaine et al., (2011) and normalized values to interglacial temperatures based on the tropical SST stack (Herbert et al., 2010) as a reference record of cave air temperature variability. We used the paleotemperature isotopic sensitivity by Tremaine et al. (2011) because this equation applies to a broad range of temperature and cave environments. The Katún $\delta^{18}O$ record after removing the temperature effect (hereafter, $Katún_{adj}$), is presented in Figure 23 and a cross-correlation analysis was applied between $Katún_{adj}$ and the composite atmospheric CO_2 record (Fig. 24). As expected from the temperature isotopic sensitivity and the glacial-interglacial tropical SST variability, temperatures have a modest influence on stalagmite $\delta^{18}O$ of about 0.5‰ during glacial intervals when temperatures were 3°C colder. Correlation analyses between $Katún_{adj}$ and the atmospheric CO_2 record over the time intervals 198-245 ky BP and 275-320 ky BP suggest a statistically

significant relationship between the time series (Pearson r = -0.23 and -0.4, for these time intervals, respectively). The correlation between $Katún_{adj}$ and tropical SSTs also is significant r = -0.4, CI 95%, p=-0.6, -0.1). These results indicate that the Katún $\delta^{18}O$ record still retains a statistically significant relationship with atmospheric CO_2 and tropical SSTs after extracting the cave air temperature component. This suggests that there is a compelling link between atmospheric greenhouse forcing and hydroclimate variability in the YP and likely in the broader Caribbean region on glacial-interglacial time scales. These results contrast with those from other monsoonal regions where hydroclimate variability is driven by the effect of climatic precession on local insolation changes, such as in the Asian and Borneo monsoon regions. We speculate that the direct effect of tropical SSTs on local hydroclimate in association with the absence of a large landmass and the geographic setting of the YP whereby it is surrounded by ocean on three directions prevents local hydroclimate to respond coherently to shifts in seasonal insolation driven by climatic precession.

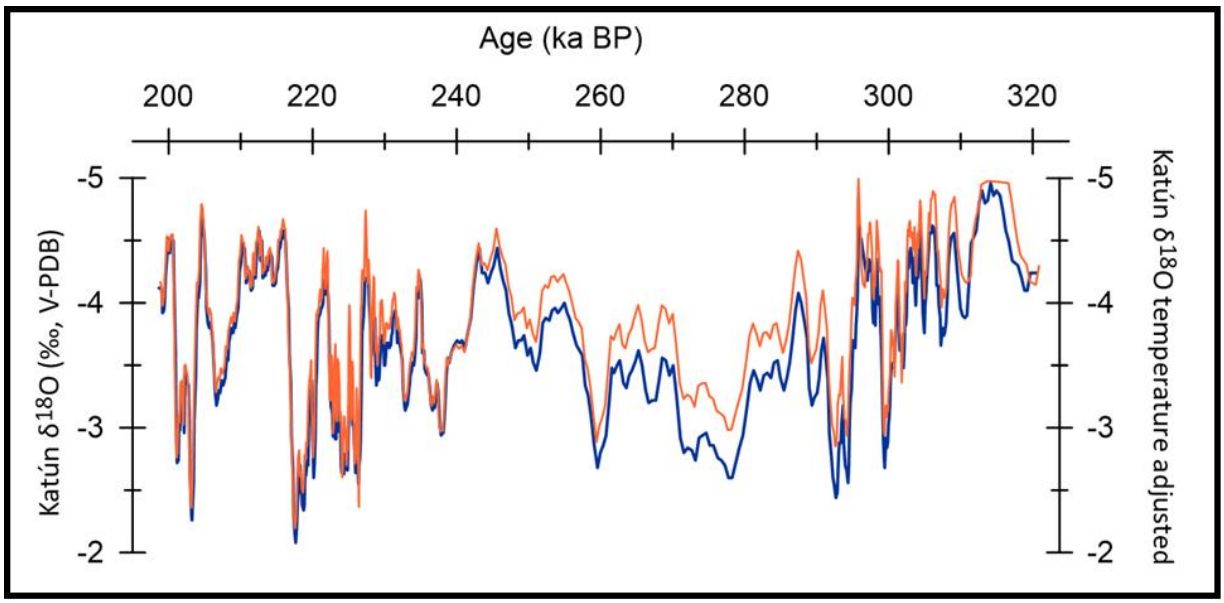

Figure 23) Katún $\delta^{18}O$ record (blue) and $Katún_{adj}$ (orange). Visually, there is not much influence from cave air temperature during wet interglacial intervals, but cave air temperatures do have a modest influence during glacial intervals.

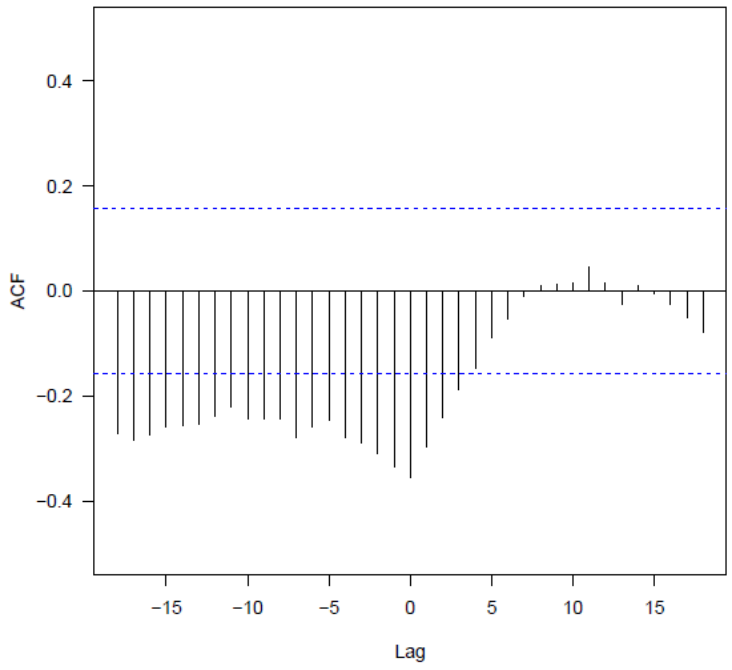

Figure 24) Cross-correlation analyses between $Katún_{adj}$ and the EPICA Dome C ice core record of pCO_2 by Lüthi et al. (2004) interpolated at 800 years with r = 0.21.

4. Conclusions

This study has produced a new stalagmite $\delta^{18}O$ record, named Katún, from the Yucatan Peninsula that spans a full glacial-interglacial interval between 322 and 198 kyr BP. We interpret the Katún $\delta^{18}O$ record to reflect the dominant precipitation amount effect in the Yucatan Peninsula as determined by previous studies (Lases-Hernandez et al., 2018; Medina-Elizalde et al., 2017). MIS 9 through 7 in marine sediment records (Lisiecki and Raymo, 2005) are identified in the new stalagmite record. In the Yucatan Peninsula interglacials are interpreted to be wet as reflected by negative stalagmite $\delta^{18}O$ values, whereas glacials are interpreted to be dry as reflected by stalagmite positive $\delta^{18}O$ values. The Katún record also shows that the amplitude of precipitation variability increases from warm interglacial to cold glacial intervals, which indicates a propensity for drought in the Caribbean during glacial conditions. Millennial-scale variability is identified within the Katún record with dominant periodicities between 4 and 8 kyr. We speculate that millennial hydroclimate variability at the time reflects shifts in AMOC, as invoked to explain millennial-scale variability in the Caribbean during the last glacial. Cross-correlation analysis results suggest that the Katún record is not strongly correlated with the precession parameter in contrast with records from deep monsoon regions such as Southeast Asia and Borneo. In contrast, we find a significant relationship between the Katún $\delta^{18}O$ record and the EPICA Dome C ice core record of atmospheric CO_2 and tropical sea surface temperatures, suggesting the atmospheric CO_2 signal enters the stalagmite paleoclimate record via tropical atmospheric surface temperature variability. Lower tropical surface temperatures are associated with lower atmospheric moisture content, a southern displacement of the ITCZ and ultimately a decrease in precipitation in the Caribbean during the last glacial. Therefore, we suggest that precipitation variability in the Yucatan Peninsula, and most likely in the broader Caribbean

region, on orbital timescales was controlled by atmospheric CO_2 via changes in tropical atmospheric and ocean temperatures.

References

Alexander, M.A., Kilbourne, K.H., and Nye, J.A., 2014, Climate variability during warm and cold phases of the Atlantic Multidecadal Oscillation (AMO) 1871–2008: Journal of Marine Systems, v. 133, p. 14–26.

Arbuszewski, J.A., Demenocal, P.B., Cléroux, C., Bradtmiller, L., and Mix, A., 2013, Meridional shifts of the Atlantic intertropical convergence zone since the Last Glacial Maximum: Nature Geoscience.

Baker, P.A., Seltzer, G.O., Fritz, S.C., Dunbar, R.B., Grove, M.J., Tapia, P.M., Cross, S.L., Rowe, H.D., and Broda, J.P., 2001, The history of South American tropical precipitation for the past 25,000 years: Science, v. 291, p. 640–643.

Bond, G., 2009, Millennial Climate Variability, In: Gornitz V. (eds) Encyclopedia of Paleoclimatology and Ancient Environments. Encyclopedia of Earth Sciences Series. Springer, Dordrecht.

Braconnot, P., Harrison, S., Joussaume, S., Peterchmitt, J., and Crucifix, M., 2007, of the Past Results of PMIP2 coupled simulations of the Mid-Holocene and Last Glacial Maximum – Part 1 : experiments and large-scale features: , p. 261–277.

Breitenbach, S.F.M., Rehfeld, K., Goswami, B., Baldini, J.U.L., Ridley, H.E., Kennett, D.J., Prufer, K.M., Aquino, V. V., Asmerom, Y., Polyak, V.J., Cheng, H., Kurths, J., and Marwan, N., 2012, Constructing proxy records from age models (COPRA): Climate of the Past, v. 8, p. 1765–1779.

Broecker, W.S., and Denton, G.H., 1990, The role of ocean-atmosphere reorganizations in glacial cycles: Quaternary Science Reviews, v. 9, p. 305–341.

Burns, S.J., Fleitmann, D., Mudelsee, M., Neff, U., Matter, A., and Mangini, A., 2002, A 780-year annually resolved record of Indian Ocean monsoon precipitation from a speleothem from south Oman: Journal of Geophysical Research D: Atmospheres, v. 107.

Carolin, S.A., Cobb, K.M., Lynch-Stieglitz, J., Moerman, J.W., Partin, J.W., Lejau, S., Malang, J., Clark, B., Tuen, A.A., and Adkins, J.F., 2016, Northern Borneo stalagmite records reveal West Pacific hydroclimate across MIS 5 and 6: Earth and Planetary Science Letters, v. 439, p. 182–193.

Cheng, H., Edwards, R.L., Shen, C.-C., Polyak, V.J., Asmerom, Y., Woodhead, J., Hellstrom, J., Wang J., Y., Kong, X.G., Spötl, C., Wang, X.F., and Alexander, E.C., 2013, Improvements in 230Th dating, 230Th and 234U half-life values, and U-Th isotopic measurements by multi-collector inductively coupled plasma mass spectrometry.: Earth and Planetary Science Letters, v. 372, p. 82–91.

Cheng, H., Edwards, R.L., Sinha, A., Spötl, C., Yi, L., Chen, S., Kelly, M., Kathayat, G., Wang, X., Li, X., Kong, X., Wang, Y., Ning, Y., and Zhang, H., 2016, The Asian monsoon over the past 640,000 years and ice age terminations: Nature, v. 534, p. 640–646.

Cheng, H., Sinha, A., Cruz, F.W., Wang, X., Edwards, R.L., D'Horta, F.M., Ribas, C.C., Vuille,

M., Stott, L.D., and Auler, A.S., 2013, Climate change patterns in Amazonia and biodiversity: Nature Communications, v. 4.

Cheng, H., Sinha, A., Wang, X., Cruz, F.W., and Edwards, R.L., 2012, The Global Paleomonsoon as seen through speleothem records from Asia and the Americas: Climate Dynamics, v. 39, p. 1045–1062.

Chiang, J.C.H., Biasutti, M., and Battisti, D.S., 2003, Sensitivity of the Atlantic Intertropical Convergence Zone to Last Glacial Maximum boundary conditions: Paleoceanography, v. 18.

Chiang, J.C.H., Cheng, W., and Bitz, C.M., 2008, Fast teleconnections to the tropical Atlantic sector from Atlantic thermohaline adjustment: Geophysical Research Letters, v. 35.

Clark, P.U., 2001, Freshwater Forcing of Abrupt Climate Change During the Last Glaciation Freshwater Forcing of Abrupt Climate Change During the Last Glaciation: v. 293, p. 283–287.

CONAGUA, 2012, Servicio meteorológico nacional, México (available at: http://smn.cna.gob.mx/).

Correa-Metrio, A., Bush, M.B., Cabrera, K.R., Sully, S., Brenner, M., Hodell, D.A., Escobar, J., and Guilderson, T., 2012, Rapid climate change and no-analog vegetation in lowland Central America during the last 86,000 years: Quaternary Science Reviews, v. 38, p. 63–75.

Cruz, F.W., Burns, S.J., Karmann, I., Sharp, W.D., Vuille, M., Cardoso, A.O., Ferrari, J.A., Silva Dias, P.L., and Viana, O., 2005, Insolation-driven changes in atmospheric circulation over the past 116,000 years in subtropical Brazil: Nature: Letters to Nature, v. 434, p. 63–66.

Dansgaard, W., Johnsen, S.J., Clausen, H.B., Dahl-Jensen, D., Gundestrup, N., Hammer, C.U., and Oeschger, H., 1984, North Atlantic climatic oscillations revealed by deep Greenland ice cores: v. 29, p. 288–298.

Deplazes, G., Lückge, A., Peterson L. C., Timmermann, A., Hamann, Y., Hughen K. A., Röhl, U., Laj, C., Cane, M.A., Sigman, D.M., and Haug, G.H., 2013, Links between tropical rainfall and North Atlantic climate during the last glacial period: Nature Geoscience, v. 6, p. 213–217.

Deplazes, G., Lückge, A., Peterson, L.C., Timmermann, A., Hamann, Y., Hughen, K.A., Röhl, U., Laj, C., Cane, M.A., Sigman, D.M., and Haug, G.H., 2013, Links between tropical rainfall and North Atlantic climate during the last glacial period: v. 6, p. 213–217.

Dorale, J.A., and Liu, Z., 2009, Limitations of hendy test criteria in judging the paleoclimatic suitability of speleothems and the need for replication: Journal of Cave and Karst Studies, v. 71, p. 73–80.

Escobar, J., Hodell, D.A., Brenner, M., Curtis, J.H., Gilli, A., Mueller, A.D., Anselmetti, F.S., Ariztegui, D., Grzesik, D.A., Pérez, L., Schwalb, A., and Guilderson, T.P., 2012, A ~43-ka record of paleoenvironmental change in the Central American lowlands inferred from stable isotopes of lacustrine ostracods: Quaternary Science Reviews, v. 37, p. 92–104.

Fensterer, C., Scholz, D., Hoffmann, D., Spötl, C., Schröder-Ritzrau, A., Horn, C., Pajon, J.,

Mangini, A., 2013, Millennial-scale climate variability during the last 12.5 ka recorded in a Caribbean speleothem. Earth and Planetary Science Letters. 361. p. 143–151.

Folland, C. K., Renwick, J. A., Salinger, M. J., Mullan A. B., 2002, Relative influences of the Interdecadal Pacific Oscillation and ENSO on the South Pacific Convergence Zone. Geophysics Research Letters, 29.

Goldenberg, S.B., Landsea, C.W., Mestas-Nuñez, A.M., and Gray, W.M., 2001, The recent increase in Atlantic hurricane activity: Causes and implications: Science, v. 293, p. 474–479.

Goldenberg, S.B., and Shapiro, L.J., 1996, Physical mechanisms for the Association of El Niño and West African rainfall with Atlantic Major Hurricane Activity: Journal of Climate, v. 9, p. 1169–1187.

Gondwe, B.R.N., Lerer, S., Stisen, S., Marín, L., Rebolledo-Vieyra, M., Merediz-Alonso, G., and Bauer-Gottwein, P., 2010, Hydrogeology of the south-eastern Yucatan Peninsula: New insights from water level measurements, geochemistry, geophysics and remote sensing: Journal of Hydrology, v. 389, p. 1–17.

Gray, W.M., 1984, Atlantic seasonal hurricane frequency. Part I: El-Niño and 30-MB quasi-biennial oscillation influences: Monthly Weather Review, v. 112, p. 1649–1688.

Gray, S.T., Graumlich, L.J., Betancourt, J.L., and Pederson, G.T., 2004, A tree-ring based reconstruction of the Atlantic Multidecadal Oscillation since 1567 A.D.: Geophysical Research Letters, v. 31.

Haug, G.H., Gunther, D., Peterson, L.C., Sigman, D.M., Hughen, K.A., and Aeshlimann, B., 2003, Climate and the Collapse of Maya Civilization: Science, v. 299, p. 1731–1735.

Hendy, C.H., 1971, The isotopic geochemistry of speleothems-I. The calculation of the effects of different modes of formation on the isotopic composition of speleothems and their applicability as palaeoclimatic indicators: Geochimica et Cosmochimica Acta, v. 35, p. 801–824.

Hendy, I.L., and Kennett, J.P., 2000, Dansgaard-Oeschger cycles and the California Current System: Planktonic foraminiferal responses to rapid climate change in Santa Barbara Basin, Ocean Drilling Program hole 893A: Paleoceanography, v. 15, p. 30–42.

Held, I. M., and B. J. Soden, 2006, Robust responses of the hydrological cycle to global warming. Journal of Climotology, 19, 5686–5699.

van Hengstum, P.J., Reinhardt, E.G., Beddows, P.A., and Gabriel, J.J., 2010, Linkages between Holocene paleoclimate and paleohydrogeology preserved in a Yucatan underwater cave: Quaternary Science Reviews, v. 29, p. 2788–2798.

Herbert, T.D., Peterson, L.C., Lawrence, K.T., and Liu, Z., 2010, Tropical Ocean Temperatures Over the Past 3.5 Million Years: Science, v. 328, p. 1530–1535.

Hodell, D.A., Anselmetti, F.S., Ariztegui, D., Brenner, M., Curtis, J.H., Gilli, A., Grzesik, D.A., Guilderson, T.J., Müller, A.D., Bush, M.B., Correa-Metrio, A., Escobar, J., and Kutterolf, S., 2008a, An 85-ka record of climate change in lowland Central America: Quaternary

Science Reviews, v. 27, p. 1152–1165

Hodell, D.A., Channeil, J.E.T., Curtis, J.H., Romero, O.E., and Röhl, U., 2008, Onset of "Hudson Strait" Heinrich events in the eastern North Atlantic at the end of the middle Pleistocene transition (~640 ka)? Paleoceanography, v. 23, p. 1–16.

Kanner, L.C., Burns, S.J., Cheng, H., and Edwards, R.L., 2012, High-latitude forcing of the South American summer monsoon during the last glacial: Science, v. 335, p. 570–573.

Karmalkar, A. V., Bradley, R.S., and Diaz, H.F., 2011, Climate change in Central America and Mexico: Regional climate model validation and climate change projections: Climate Dynamics, v. 37, p. 605–629, doi: 10.1007/s00382-011-1099-9.

Knight, J.R., Folland, C.K., and Scaife, A.A., 2006, Climate impacts of the Atlantic Multidecadal Oscillation: Geophysical Research Letters, v. 33.

Krebs, U., and Timmermann, A., 2007, Tropical Air–Sea Interactions Accelerate the Recovery of the Atlantic Meridional Overturning Circulation after a Major Shutdown: Journal of Climate, v. 20, p. 4940–4956.

Kutzbach, J.E., and Guetter, P.J., 1986, The Influence of changing Orbital Parameter and Surface Boundary Conditions on Climate Simulations for the Past 18,000 Years: Journal of Atmospheric Sciences, v. 43, p. 1726–1759.

Lachniet, M.S., 2009, Climatic and environmental controls on speleothem oxygen-isotope values: Quaternary Science Reviews, v. 28, p. 412–432.

Lachniet, M.S., and Patterson, W.P., 2009, Oxygen isotope values of precipitation and surface waters in northern Central America (Belize and Guatemala) are dominated by temperature and amount effects: Earth and Planetary Science Letters, v. 284, p. 435–446.

Lambert, J.W., and Aharon, P., 2010, Oxygen and hydrogen isotopes of rainfall and dripwater at SeSoto Caverns (Alabama, USA); Key to understanding past variability of moisture transport from the Gulf of Mexico: Geochimica et Cosmochimica Acta, v. 74, p. 846–861.

Larson, J., Zhou, Y., and Higgins, W.R., 2005, Characteristics of Landfalling Tropical Cyclones in the United States and Mexico: Climatology and Interannual Variability: Journal of Climate, v. 18.

Lases-hernandez, F., Medina-elizalde, M., Burns, S., and Decesare, M., 2018, Long-term monitoring of drip water and groundwater stable isotopic variability in the Yucatán Peninsula: Implications for recharge and speleothem rainfall reconstruction: Geochimica et Cosmochimica Acta, v. 246, p. 41–59.

Lewis, S.C., Legrande, A.N., Kelley, M., and Schmidt, G.A., 2010, Water vapour source impacts on oxygen isotope variability in tropical precipitation during Heinrich events: Climate of the Past, v. 6, p. 325–343.

Lisiecki, L.E., and Raymo, M.E., 2005, A Pliocene-Pleistocene stack of 57 globally distributed benthic delta O-18 records: Paleoceanography, v. 20.

Lopez-Ramos, E., 1975. Geological summary of the Yucatan Peninsula. In: Nairn, A.E.M.,

Stehli, F.G. (Eds.), The Ocean Basins and Margins, The Gulf of Mexico and the Caribbean, vol. 3. Plenum Press, NY, USA (Chapter 7).

Lui, Y., San Liang, X., and Weisberg, R.H., 2007, Rectification of the bias in the wavelet power spectrum: Journal of Atmospheric and Oceanic Technology, v. 24, p. 2093–2109.

Lüthi, D., Le Floch, M., Bereiter, B., Blunier, T., Barnola, J.M., Siegenthaler, U., Raynaud, D., Jouzel, J., Fischer, H., Kawamura, K., and Stocker, T.F., 2008, High-resolution carbon dioxide concentration record 650,000-800,000 years before present: Nature, v. 453, p. 379–382.

Magaña, V., Amador, J.A., and Medina, S., 1999, The midsummer drought over Mexico and Central America: Journal of Climate, v. 12, p. 1577–1588.

Magaña, V.O., V azquez, J.L., P erez, J.L., and P erez, J.B., 2003, Impact of el niño on precipitation in Mexico: Geofis. Internacional-Mexico, v. 42, p. 313–330.

Meckler, A.N., Clarkson, M.O., Cobb, K.M., Sodemann, H., and Adkins, J.F., 2012, Interglacial hydroclimate in the tropical West Pacific through the late pleistocene: Science, v. 336, p. 1301–1304.

Medina-Elizalde, M., Burns, S.J., Lea, D.W., Asmerom, Y., von Gunten, L., Polyak, V., Vuille, M., and Karmalkar, A., 2010, High resolution stalagmite climate record from the Yucatán Peninsula spanning the Maya terminal classic period: Earth and Planetary Science Letters, v. 298, p. 255–262.

Medina-Elizalde, M., Polanco-Martinez, J. M., Lases-Hernandez, F., Bradley, R., and Burns, S., 2016a, Testing the "tropical storm" hypothesis of Yucatan Peninsula climate variability during the Maya Terminal Classic Period: Quaternary Research, v. 86, no. 2, p. 111-119.

Medina-Elizalde, M., Burns, S.J., Polanco-Martínez, J.M., Beach, T., Lases-Hernández, F., Shen, C.C., and Wang, H.C., 2016b, High-resolution speleothem record of precipitation from the Yucatan Peninsula spanning the Maya Preclassic Period: Global and Planetary Change.

Medina-Elizalde, M., Burns, S.J., Polanco-Martinez, J., Lases-Hernandez, F., Bradley, R., Wang, H., and Shen, C., 2017, Synchronous precipitation reduction in the American Tropics associated with Heinrich 2: Scientific Reports, v. 7: 1126, p. 1–12.

Medina-Elizalde, M., and Rohling, E.J., 2012, Collapse of Classic Maya Civilization Related to Modest Reduction in Precipitation: Science.

Mendoza, B., Velasco, V., and Jáuregui, E., 2006, A Study of historical droughts in southeastern Mexico: Journal of Climate, v. 19, p. 2916–2934.

Mestas-Nuñez, A.M., Enfield, D.B., and Zhang, C., 2007, Water vapor fluxes over the Intra-Americas Sea: Seasonal and interannual variability and associations with rainfall: Journal of Climate, v. 20, p. 1910–1922.

Mohtadi, M., Prange, M., and Steinke, S., 2016, Palaeoclimatic insights into forcing and response of monsoon rainfall: Nature, v. 533, p. 191–199.

Moura, A.D., and Shukla, J., 1981, On the dynamics of droughts in northeast Brazil:

Observations, theory and numerical experiments with a general circulation model: Journal of Atmospheric Science, v. 38, p. 2653–2675.

Munoz, E., Busalacchi, A.J., Nigam, S., and Ruiz-Barradas, A., 2008, Winter and summer structure of the Caribbean low-level jet: Journal of Climate, v. 21, p. 1260–1276.

Oeschger, H., Beer, J., Siegenthaler, U., Stauffer, B., Dansgaard, W., and Langwat, C.C., 1984, Late Glacial climate history from ice cores: Geophysical Monographs, v. 29, p. 299–306.

Otto-Bliesner, B.L., and Brady, E.C., 2010, The sensitivity of the climate response to the magnitude and location of freshwater forcing: last glacial maximum experiments: Quaternary Science Reviews, v. 29, p. 56–73.

Otto-bliesner, B.L., Russell, J.M., Clark, P.U., Liu, Z., Overpeck, J.T., Konecky, B., Nicholson, S.E., He, F., and Lu, Z., 2014, Coherent changes of southeastern equatorial and northern African rainfall during the last deglaciation: Science, v. 346, p. 1223–1227.

Palaeosens, P. M., 2012, Making sense of palaeoclimate sensitivity: Nature, v. 491, p. 683-691.

Patricola, C.M., and Cook, K.H., 2007, Dynamics of the West African monsoon under mid-Holocene precessional forcing: Regional climate model simulations: Journal of Climate, v. 20, p. 694–716.

Peterson, L.C., and Haug, G.H., 2006, Variability in the mean latitude of the Atlantic Intertropical Convergence Zone as recorded by riverine input of sediments to the Cariaco Basin (Venezuela): Palaeogeography Palaeoclimatology Palaeoecology, v. 234, p. 97–113.

Peterson, L.C., Haug, G.H., Hughen, K.A., and Röhl, U., 2000, Rapid Changes in the Hydrologic Cycle of the Tropical Atlantic During the Last Glacial: Science, v. 290, p. 1947–1951.

Rahmstorf, S., 2002, Ocean circulation and climate during the past 120,000 years: Nature, v. 419, p. 207–214.

Rohling, E.J., Sluijs, A., Dijkstra, H.A., Kohler, P., de Wal, R.S.W. V, von der Heydt, A.S., Beerling, D.J., Berger, A., Bijl, P.K., Crucifix, M., DeConto, R., Drijfhout, S.S., Fedorov, A., Foster, G.L., et al., 2012, Making sense of palaeoclimate sensitivity: Nature, v. 491, p. 683–691.

Rozanski, K., Araguás-Araguás, L., and Gonfiantini, R., 1993, Isotopic Patterns in Modern Global Precipitation: , p. 1–36, doi: 10.1029/GM078p0001.

Schönian, F., Stöffler, D., Kenkmann, T., Wittmann, A., 2004. The fluidized Chicxulub ejecta blanket, Mexico: implications for Mars. Poster. In: 35th Annu. Lunar and Planet. Sci. Conf., League City, TX, USA.

Shackleton, N.J., 2000, The 100,000-Year Ice-Age Cycle Identified and Found to Lag Temperature , Carbon Dioxide, and Orbital Eccentricity: Science: Research Articles, v. 289, p. 1897–1902.

SGM, 2007, Carta geológica de México. Escala 1:2000,000. 6a edición. Servicio Geológico Mexicano (SGM).

Shaw, C.E., 2016, Late Pleistocene Bays and Reefs : Ancestors to the Modern Caribbean Coast ,

Late Pleistocene Bays and Reefs : Ancestors to the Modern ´ n Pen ´ Caribbean Coast , Yucata ınsula , M ´ exico: Journal of Coastal Research, v. 32, p. 280–285.

Shen, C.-C., Cheng, H., Edwards, R.L., Moran, S.B., Edmonds, H.N., Hoff, J.A., and Thomas, R.B., 2003, Measurement of attogram quantities of 231Pa in dissolved and particulate fractions of seawater by isotope dilution thermal ionization mass spectroscopy: Analytical Chemistry , v. 75, p. 1075–1079.

Shen, C.-C., Edwards, R.L., Cheng, H., Dorale, J.A., Thomas, R.B., Moran, S.B., Weinstein, S.E., and Edmonds, H.N., 2002, Uranium and thorium isotopic and concentration measurements by magnetic sector inductively coupled plasma mass spectrometry: Chem. Geol., v. 185, p. 165–178.

Shen, C.C., Wu, C.C., Cheng, H., Lawrence Edwards, R., Hsieh, Y. Te, Gallet, S., Chang, C.C., Li, T.Y., Lam, D.D., Kano, A., Hori, M., and Spötl, C., 2012, High-precision and high-resolution carbonate230Th dating by MC-ICP-MS with SEM protocols: Geochimica et Cosmochimica Acta, v. 99, p. 71–86.

Stouffer, R.J., Broccoli, A.J., Delworth, T.L., Dixon, K.W., Gudgel, R., Held, I., Hemler, R., Knutson, T., Lee, H.C., Schwarzkopf, M.D., Soden, B., Spelman, M.J., Winton, M., and Zeng, F., 2006, GFDL's CM2 global coupled climate models. Part IV: Idealized climate response: Journal of Climate, v. 19, p. 723–740.

Stouffer, R.J., Yin, J., Gregory, J.M.J.M., Dixon, K.W., Spelman, M.J., Hurlin, W., Weaver, a. J., Eby, M., Flato, G.M., Hasumi, H., Hu, A., Jungclaus, J.H., Kamenkovich, I. V., Levermann, A., et al., 2006, Investigating the causes of the response of the thermohaline circulation to past and future climate changes.: Journal of Climate, v. 19, p. 1365–1387.

Torrence, C., and Compo, G.P., 1998, A practical guide to wavelet analysis: Bulletin of the American Meteorological Society, v. 79, p. 61–78.

Tremaine, D.M., Froelich, P.N., Wang, Y., 2011. Speleothem calcite farmed in situ: modern calibration of delta O-18 and delta C-13 paleoclimate proxies in a continuously-monitored natural cave system. Geochim. Cosmochim. Acta 75, p. 4929-4950.

USGS, 2006, Shuttle Radar Topography Mission, 3 Arc Second, Finished 2.0. Global Land Cover Facility, University of Maryland, College Park, MD, USA.

Vuille, M., Bradley, R.S., Healy, R., Werner, M., Hardy, D.R., Thompson, L.G., and Keimig, F., 2003, Modeling δ 18 O in precipitation over the tropical Americas: 2. Simulation of the stable isotope signal in Andean ice cores: Journal of Geophysical Research, v. 108, p. 4175.

Wang, Y.J., Cheng, H., Edwards, R.L., An, Z.S., Wu, J.Y., Shen, C.C., and Dorale, J.A., 2001, A high-resolution absolute-dated late pleistocene monsoon record from Hulu Cave, China: Science, v. 294, p. 2345–2348.

Wang, Y., Cheng, H., Edwards, R.L., Kong, X., Shao, X., Chen, S., Wu, J., Jiang, X., Wang, X., and An, Z., 2008, Millennial- and orbital-scale changes in the East Asian monsoon over the past 224,000[thinsp]years: Nature, v. 451, p. 1090–1093.

Weidie, A.E., 1985. Part I. Geology of Yucata´n Platform. In: Ward, W.C.; Weidie, A.E., and Back, W. (eds.), Geology and Hydrogeology of the Yucatan and Quaternary Geology of the

Northeastern Yucatan Peninsula. New Orleans, Louisiana: New Orleans Geological Society, 1–19.

Table 1) U-Th dates for speleothem Katún.

U-Th dates from speleothem Katún												
Sample	Distance	Weight	^{238}U		^{232}Th		$\delta^{234}U$		$[^{230}Th/^{232}Th]$		Age	
ID	mm	g	ppb[a]		ppt		measured[b]		ppm[d]		corrected[c,e]	
K3-5	160	0.16689	79.7	± 0.07	322.9	± 2.8	22.5	± 1.1	3507	± 31	198,687	± 1422
K3-6	228	0.12098	86.22	± 0.09	107	± 3.8	24.8	± 1.2	11876	± 426	219,978	± 1726
K3-9	530	0.0787	319.93	± 0.45	444.6	± 5.9	19.1	± 1.6	11384	± 152	299,742	± 4438
L8	175	0.1799	286.23	± 0.52	662.4	± 2.9	23.1	± 2.2	6208	± 29	204,680	± 2149
L11	300	0.15798	90.09	± 0.26	46	± 2.9	26.5	± 2.9	29336	± 1877	229,592	± 3758
L12	388	0.13927	436.05	± 0.67	3024.6	± 9.2	23.7	± 1.7	2227.8	± 9.2	261,743	± 4087
L13	462	0.17108	293.94	± 0.38	903.8	± 3.2	22.9	± 1.4	5147	± 21	293,026	± 4263
L15	608	0.17443	173.3	± 0.20	501.7	± 2.8	22.6	± 1.3	5519	± 32	308,611	± 4216
L16	644	0.21146	162.78	± 0.23	246.1	± 2.3	18.9	± 1.6	10600	± 100	322,775	± 5978

Analytical errors are 2σ of the mean.

[a] $\delta^{234}U = ([^{234}U/^{238}U]_{activity} - 1) \times 1000$.

[b] $\delta^{234}U_{initial}$ corrected was calculated based on ^{230}Th age (T), i.e., $\delta^{234}U_{initial} = \delta^{234}U_{measured} \times e^{\lambda 234 * T}$, and T is corrected age.

[c] $[^{230}Th/^{238}U]activity = 1 - e^{-\lambda 230 T} + (\delta^{234}U_{measured}/1000)[\lambda_{230}/(\lambda_{230} - \lambda_{234})](1 - e^{-(\lambda 230 - \lambda 234) T})$, where T is the age.

Decay constants are 9.1577×10^{-6} yr^{-1} for ^{230}Th, 2.8263×10^{-6} yr^{-1} for ^{234}U (Cheng et al., 2000), and 1.55125×10^{-10} yr^{-1} for ^{238}U (Jaffey et al., 1971).

[d] Age (relative to chemistry date of July 2012) corrections were calculated using an $^{230}Th/^{232}Th$ atomic ratio of 4 (± 2) ppm.

Those are the values for a material at secular equilibrium, with the crustal $^{232}Th/^{238}U$ value of 3.8. The errors are arbitrarily assumed to be 50%.

[e] $\delta^{234}U_{initial}$ corrected was calculated based on ^{230}Th age (T), i.e., $\delta^{234}U_{initial} = \delta^{234}U_{measured} \times e^{\lambda 234 * T}$, and T is corrected age.

Table 2) Ages, $\delta^{18}O$, and $\delta^{13}C$ associated with stalagmite depth.

Depth from top (mm)	Age (yr BP)	$\delta^{18}O$	$\delta^{13}C$
160	198671.1	-4.18	-2.09
160.5	198879.1	-4.91	-3
161	199086.5	-4.1	-2.47
161.5	199293.3	-3.95	-1.99
162	199499.6	-3.49	-2.5
162.5	199705.2	-4.04	-2.55
163	199910.3	-4.09	-2.37
163.5	200114.8	-4.19	-2.58
164	200318.6	-4.27	-2.61
164.5	200521.9	-4.35	-2.71
165	200724.6	-4.79	-3.34
165.5	200926.6	-4.88	-3.27
166	201128.1	-3.86	-2.11
166.5	201328.9	-4.01	-1.15
167	201529.1	-4.78	-2.21
167.5	201728.7	-4.95	-3.81
168	201927.6	-4.9	-3.09
168.5	202125.9	-3.87	-0.95
169	202323.5	-2.22	0.87
169.5	202520.6	-2.16	2.06
170	202716.9	-1.78	1.11
170.5	202912.6	-3.46	-0.75
171	203107.7	-4.04	-1.03
171.5	203302.1	-3.72	-1.09
172	203495.8	-1.85	1.17
172.5	203688.8	-3.32	-0.34
173	203881.2	-3.56	-0.92
173.5	204072.9	-3.15	0.12
174	204263.9	-2.83	0.62
174.5	204454.2	-4.18	-1.24
175	204643.9	-3.37	-0.64
175.5	204832.8	-3.27	-0.58
176	205021.0	-2.99	0.03
176.5	205208.5	-1.81	1.46
177	205395.4	-1.67	1.96
177.5	205581.5	-1.83	2.75
178	205766.8	-3.01	0.84
178.5	205951.5	-4.49	-2.47

179	206135.4	-4.28	-1.58
179.5	206318.6	-3.43	-0.01
180	206501.1	-3.71	-1.78
180.5	206682.8	-4.39	-1.63
181	206863.8	-4.41	-0.61
181.5	207044.1	-4.86	-1.68
182	207223.6	-5.22	-1.84
182.5	207402.3	-4.55	-2.12
183	207580.3	-4.24	-1.79
183.5	207757.5	-3.76	-0.36
184	207933.9	-3.49	-0.75
184.5	208109.6	-3.84	-0.74
185	208284.4	-3.95	-1.05
185.5	208458.5	-3.98	-1.08
186	208631.9	-3.99	-0.87
186.5	208804.4	-3.29	-0.25
187	208976.1	-3.16	-0.49
187.5	209147.0	-3.21	-0.92
188	209317.2	-2.84	-1.45
188.5	209486.5	-3.39	-1.82
189	209655.0	-3.56	-1.71
189.5	209822.7	-3.49	-1.41
190	209989.6	-3.1	-1.49
190.5	210155.6	-3.32	-1.83
191	210320.8	-3.16	-2.35
191.5	210485.2	-3.72	-2.79
192	210648.8	-3.67	-2.78
192.5	210811.5	-3.92	-2.11
193	210973.3	-3.23	-1.48
193.5	211134.3	-3.93	-2.54
194	211294.5	-3.95	-2.9
194.5	211453.8	-4	-2.02
195	211612.2	-3.7	-1.94
195.5	211769.8	-3.66	-2.32
196	211926.5	-3.61	-2.38
196.5	212082.3	-4.55	-2.22
197	212237.3	-4.31	-2.09
197.5	212391.3	-5.24	-2.79
198	212544.5	-3.97	-2.13
198.5	212696.7	-4.39	-2.28
199	212848.1	-4.32	-2.18

199.5	212998.6	-4.26	-1.78
200	213148.2	-3.82	-0.83
200.5	213296.8	-4.17	-0.81
201	213444.6	-4.7	-0.75
201.5	213591.4	-3.97	-0.36
202	213737.3	-3.77	-0.3
202.5	213882.3	-3.9	-0.98
203	214026.3	-5.46	-1.84
203.5	214169.4	-3.82	-1.7
204	214311.6	-5.27	-3.55
204.5	214452.8	-3.88	-3.41
205	214593.1	-4.42	-3.48
205.5	214732.4	-4.3	-2.98
206	214870.8	-4.58	-3.42
206.5	215008.2	-3.78	-3.53
207	215144.7	-4.03	-4.06
207.5	215280.1	-4.41	-4.44
208	215414.6	-4.84	-4.42
208.5	215548.1	-4.26	-4.06
209	215680.7	-4.29	-4.09
209.5	215812.2	-4.18	-4.41
210	215942.8	-4.16	-4.39
210.5	216072.4	-3.68	-3.88
211	216200.9	-4.27	-4.64
211.5	216328.5	-4.44	-4.73
212	216455.0	-4.56	-5.15
212.5	216580.6	-4.4	-4.64
213	216705.1	-4.58	-4.66
213.5	216828.6	-4.23	-4.21
214	216951.1	-4.81	-4.4
214.5	217072.5	-4.63	-5.24
215	217193.0	-4.75	-5.44
215.5	217312.3	-4.29	-3.56
216	217430.7	-4.06	-1.35
216.5	217548.0	-3.03	0.33
217	217664.2	-3.73	-0.33
217.5	217779.4	-2.95	0.91
218	217893.5	-3.1	2.08
218.5	218006.6	-2.15	3.09
219	218118.6	-1.59	3.37
219.5	218229.5	-1.84	2.9

220	218339.3	-2.06	2.21
220.5	218448.1	-2.8	1.61
221	218555.8	-2.6	1.74
221.5	218662.4	-3	2.96
222	218767.9	-2.77	2.93
222.5	218872.3	-2.34	3.48
223	218975.6	-1.75	2.06
223.5	219077.8	-2.72	0.6
224	219178.8	-2.37	0.92
224.5	219278.8	-2.58	0.49
225	219377.7	-2.53	0.19
225.5	219475.4	-3.04	-0.21
226	219572.0	-2.55	0.36
226.5	219667.4	-3.04	-0.17
227	219761.8	-2.41	1.01
227.5	219855.0	-3.98	1.9
228	219947.0	-3.79	1.72
228.5	220037.9	-3.04	2.12
229	220127.7	-3.23	3.3
229.5	220216.3	-2.92	3.14
230	220303.9	-2.14	2.25
230.5	220390.4	-2.81	1.96
231	220475.8	-1.95	2.09
231.5	220560.1	-3.76	0.42
232	220643.5	-3.85	-1.08
232.5	220725.8	-4.19	-2.16
233	220807.1	-3.9	-1.6
233.5	220887.5	-3.06	-1.82
234	220966.8	-3.51	-1.21
234.5	221045.3	-4.25	-0.17
235	221122.8	-4.04	0.09
235.5	221199.4	-4.16	-0.23
236	221275.1	-3.44	0.93
236.5	221349.9	-3.8	0.76
237	221423.9	-3.74	-1.2
237.5	221497.0	-4.25	-2.12
238	221569.3	-4.07	-2.71
238.5	221640.8	-4.55	-2.98
239	221711.5	-3.98	-3.02
239.5	221781.4	-4.45	-4.98
240	221850.5	-3.57	-3.93

240.5	221919.0	-4.06	-3.5
241	221986.6	-3.58	-2.58
241.5	222053.6	-4.58	-3.27
242	222119.9	-4.11	-3.44
242.5	222185.5	-4.61	-1.39
243	222250.5	-4.24	-0.9
243.5	222314.8	-3.23	-0.24
244	222378.5	-2.62	-2.09
244.5	222441.6	-3.43	-1.75
245	222504.1	-2.8	-1.62
245.5	222566.0	-3.04	-2.83
246	222627.3	-3.22	-1.4
246.5	222688.2	-4.4	-1.94
247	222748.5	-3.09	-3.45
247.5	222808.3	-3.15	-2.91
248	222867.6	-2.59	-2.01
248.5	222926.4	-3.04	-2.63
249	222984.8	-1.91	-1.15
249.5	223042.8	-3.23	-2.19
250	223100.3	-3.64	-1.48
250.5	223157.4	-4.27	-1.96
251	223214.2	-3.75	-0.82
251.5	223270.5	-2.43	-1.47
252	223326.5	-2.72	-2.18
252.5	223382.2	-2.92	-2.22
253	223437.6	-3.08	-2.49
253.5	223492.7	-3.06	-1.82
254	223547.4	-2.87	-3.02
254.5	223601.9	-4.76	-3.2
255	223656.2	-2.73	-2.52
255.5	223710.2	-3.14	-3.11
256	223764.0	-2.43	-2.78
256.5	223817.6	-2.76	-3.49
257	223871.1	-3.13	-3.98
257.5	223924.3	-3.11	-3.85
258	223977.4	-3.08	-3.29
258.5	224030.4	-2.2	-2.98
259	224083.2	-1.7	-2.16
259.5	224136.0	-2.08	0.47
260	224188.7	-2.85	-0.94
260.5	224241.3	-3.12	-1.66

261	224293.9	-2.85	-1.67
261.5	224346.4	-2.37	-1.5
262	224398.9	-2.81	-2.45
262.5	224451.5	-3.17	-3.26
263	224504.0	-3.06	-4.04
263.5	224556.6	-2.44	-1.95
264	224609.2	-2.44	-1.46
264.5	224661.9	-2.33	-0.54
265	224714.7	-3.46	-2.12
265.5	224767.6	-1.68	-1.58
266	224820.6	-2.43	-2.77
266.5	224873.8	-3.03	-2.68
267	224927.1	-2.63	-0.15
267.5	224980.6	-3.17	-0.59
268	225034.3	-2.98	-2.85
268.5	225088.2	-5.23	-2.25
269	225142.3	-4.09	-3.08
269.5	225196.6	-3.25	-3.17
270	225251.2	-2.88	-2.86
270.5	225306.1	-2.19	-3.89
271	225361.3	-2.86	-5.13
271.5	225416.7	-2.95	-5.8
272	225472.5	-3.45	-5.88
272.5	225528.7	-3.76	-5.48
273	225585.2	-3.26	-5.37
273.5	225642.1	-3.04	-6.49
274	225699.3	-2.72	-5.6
274.5	225757.0	-2.72	-4.69
275	225815.1	-2.61	-4.52
275.5	225873.7	-2.21	-4.88
276	225932.7	-2.33	-3.94
276.5	225992.2	-2.67	-3.47
277	226052.2	-2.54	-4.23
277.5	226112.7	-2.99	-5.48
278	226173.7	-2.85	-5.4
278.5	226235.2	-3.02	-4.74
279	226297.4	-3.99	-4.81
279.5	226360.1	-2.1	-3.99
280	226423.4	-2.15	-3.39
280.5	226487.3	-1.74	-4.26
281	226551.9	-2.04	-3.28

281.5	226617.0	-2.59	-2.86
282	226682.9	-4.36	-4.17
282.5	226749.4	-3.18	-4.45
283	226816.7	-3.36	-5.02
283.5	226884.6	-4.1	-5.41
284	226953.3	-3.69	-4.16
284.5	227022.7	-4.2	-4.73
285	227092.9	-4.39	-5.27
285.5	227163.9	-3.72	-3.99
286	227235.7	-3.85	-4.69
286.5	227308.3	-3.6	-4.34
287	227381.7	-4.33	-4.14
287.5	227456.0	-4.19	-5.38
288	227531.1	-4.78	-5.84
288.5	227607.2	-4.9	-4.98
289	227684.1	-4.27	-5.28
289.5	227761.9	-3.75	-5.41
290	227840.7	-3.42	-4.65
290.5	227920.5	-3.74	-3.85
291	228001.2	-4.39	-4.37
291.5	228082.8	-4.8	-4.38
292	228165.5	-4.16	-2.92
292.5	228249.2	-2.82	-0.78
293	228334.0	-3.25	-2.23
293.5	228419.8	-2.78	-2.85
294	228506.7	-2.95	-3.77
294.5	228594.6	-4.03	-4.28
295	228683.7	-4.96	-4.4
295.5	228773.9	-3.91	-3.04
296	228865.2	-3.32	-2.44
296.5	228957.6	-3.73	-2.54
297	229051.3	-3.97	-2.26
297.5	229146.1	-3.05	0.67
298	229242.2	-3.11	0.16
298.5	229339.4	-3.13	0.61
299	229437.9	-3.99	0.63
299.5	229537.7	-3.21	2.27
300	229638.7	-3.53	1.13
300.5	229741.0	-3.24	0.57
301	229844.6	-3.71	0.55
301.5	229949.5	-3.95	0.82

302	230055.7	-4.63	0.04
302.5	230163.1	-3.62	0.95
303	230271.8	-3.31	0.56
303.5	230381.7	-3.41	-2.4
304	230492.9	-3.32	-1.45
304.5	230605.3	-3.89	-1.91
305	230719.0	-3.63	-1.02
305.5	230833.9	-3.7	-0.14
306	230950.0	-3.88	0.31
306.5	231067.3	-3.3	0.76
307	231185.8	-3.9	0.32
307.5	231305.6	-3.44	0.3
308	231426.5	-3.78	-0.08
308.5	231548.6	-3.89	0.06
309	231672.0	-3.73	-0.92
309.5	231796.4	-4	-1
310	231922.1	-4.05	-0.55
310.5	232049.0	-3.87	-0.17
311	232177.0	-4.13	-0.73
311.5	232306.1	-3.57	-0.53
312	232436.4	-3.46	-0.45
312.5	232567.9	-3.35	-0.78
313	232700.4	-4.33	-1.53
313.5	232834.1	-3.79	-1.32
314	232969.0	-3.44	-1.21
314.5	233104.9	-3.07	-1.63
315	233242.0	-3.14	0.89
315.5	233380.2	-3.2	1.4
316	233519.4	-3.06	-0.41
316.5	233659.8	-3.16	0.02
317	233801.3	-3.29	1.21
317.5	233943.8	-3.09	0.88
318	234087.4	-3.52	1.15
318.5	234232.1	-3.63	0.93
319	234377.8	-3.57	-0.89
319.5	234524.6	-3.54	-2.23
320	234672.5	-3.41	-2.38
320.5	234821.4	-3.4	-2.39
321	234971.3	-3.9	-2.22
321.5	235122.3	-4.44	-2.12
322	235274.3	-5.16	-3.16

322.5	235427.3	-3.26	0.3
323	235581.3	-4.27	-3.33
323.5	235736.3	-3.68	-3.46
324	235892.4	-3.42	-3.46
324.5	236049.4	-3.32	-3.63
325	236207.4	-3.41	-3.82
325.5	236366.4	-3.59	-4.39
326	236526.4	-3.53	-0.94
326.5	236687.3	-3.27	1.32
327	236849.2	-3.39	1.04
327.5	237012.1	-2.84	1.5
328	237175.9	-2.94	1.74
328.5	237340.7	-3.26	0.86
329	237506.4	-3.67	-0.12
329.5	237673.1	-3.14	0.98
330	237840.6	-3.34	2.05
330.5	238009.1	-3.4	1.87
331	238178.5	-2.86	2.38
331.5	238348.8	-2.45	1.8
332	238520.1	-2.75	1.27
332.5	238692.2	-3.43	0.89
333	238865.2	-3.38	0.82
333.5	239039.1	-3.73	-2.24
334	239213.8	-3.9	-1.98
335	239566.0	-3.42	-1.05
336	239921.6	-3.17	0.54
337	240280.5	-3.83	0.72
338	240642.9	-3.96	-0.09
339	241008.5	-4.08	-0.45
340	241377.3	-3.25	1.01
341	241749.4	-3.26	1.88
342	242124.6	-3.55	-0.29
343	242502.9	-4.57	-1.82
344	242884.2	-4.72	-1.19
345	243268.5	-4.61	-1.72
346	243655.8	-4.25	-0.18
347	244046.0	-4.09	-0.11
348	244439.0	-3.59	-1.62
349	244834.8	-4.69	-1.41
350	245233.4	-4.2	-0.17
351	245634.7	-4.57	-2.2

352	246038.6	-4.35	-3.06
353	246445.1	-4.33	-1.71
354	246854.2	-3.89	-0.24
355	247265.8	-3.71	1.46
356	247679.9	-4.21	1.25
357	248096.3	-3.45	-0.05
358	248515.1	-3.83	-1.57
359	248936.3	-2.95	-0.98
360	249359.6	-3.96	-2.09
361	249785.2	-4.21	-2.99
362	250213.0	-3.66	-2.23
363	250642.8	-2.98	-1.13
364	251074.7	-3.31	-2.01
365	251508.7	-3.41	-2.22
366	251944.6	-3.88	-3.26
367	252382.4	-4.44	-4.36
368	252822.1	-4.24	-3.86
369	253263.6	-3.55	-1.51
370	253706.8	-3.3	-1.38
371	254151.8	-4.33	-1.76
372	254598.4	-4.47	-2.05
373	255046.7	-4.01	-1.14
374	255496.5	-3.73	-0.94
375	255947.9	-3.45	-0.02
376	256400.7	-3.95	0.32
377	256855.0	-4.18	-0.37
378	257310.6	-3.5	-0.46
379	257767.5	-3.24	-0.37
380	258225.8	-3.32	-0.75
381	258685.2	-3.73	-1.22
382	259145.8	-2.98	0.69
383	259607.6	-3.1	1.07
384	260070.4	-2.42	-1.74
385	260534.3	-2.18	-0.95
386	260999.1	-2.73	-1.59
387	261464.9	-3.6	-2.16
388	261931.5	-3.42	-1.22
389	262399.0	-2.83	-1.51
390	262867.2	-3.52	-1.81
391	263336.0	-4.08	-2.51
392	263805.4	-3.39	-1.71

393	264275.2	-3.71	-2.84
394	264745.4	-3.03	-3.35
395	265215.7	-2.64	-0.94
396	265686.3	-3.86	-5.03
397	266156.9	-3.86	-4.39
398	266627.4	-3.91	-3.91
399	267097.7	-3.45	-3.5
400	267567.9	-3.02	-4.4
401	268037.6	-3.25	-6.47
402	268506.9	-2.93	
403	268975.7	-3.44	2.07
404	269443.8	-3.55	-6.57
405	269911.2	-3.05	-6.69
406	270377.7	-4.18	-7.56
407	270843.3	-3.66	-5.45
408	271307.8	-3.29	-3.06
409	271771.3	-2.95	-2.53
410	272233.4	-3.42	-2.7
411	272694.2	-2.91	-2.51
412	273153.6	-2.12	-0.96
413	273611.5	-2.68	2.02
414	274067.7	-3.14	-1.61
415	274522.2	-3.32	-0.69
416	274974.9	-2.55	0.23
417	275425.6	-2.98	-1.6
418	275874.3	-2.8	-2.67
419	276320.9	-3.17	-3.16
420	276765.3	-2.82	-2.75
421	277207.3	-2.46	-2.37
422	277646.9	-2.5	-1.95
423	278084.0	-2.71	-11.08
424	278518.5	-3.04	-2.25
425	278950.3	-2.3	-2.15
426	279379.2	-2.49	-1.62
427	279805.2	-3.1	-3.16
428	280228.2	-3.26	-3.29
429	280648.2	-3.55	-4.01
430	281064.8	-3.34	-3.9
431	281478.2	-3.63	-3.32
432	281888.2	-3.61	-2.93
433	282294.7	-2.88	-11.08

434	282697.6	-3.07	-0.75
435	283096.7	-3.88	-0.67
436	283492.1	-3.69	-0.67
437	283883.5	-3.36	0.03
438	284271.0	-3.45	-0.24
439	284654.4	-3.17	-0.22
440	285033.5	-3.24	-1.52
441	285408.4	-3.17	-4.65
442	285778.9	-3.86	-5.03
443	286144.9	-4.15	-11.08
444	286506.3	-4.24	-2.44
445	286863.0	-4.34	-3.31
446	287214.9	-3.89	-4.25
447	287562.0	-3.53	-0.75
448	287904.0	-3.38	-0.63
449	288241.0	-3.47	-0.06
450	288572.8	-2.31	-0.63
451	288899.3	-3.21	-0.82
452	289220.4	-3.78	-2.06
453	289536.1	-3.58	-2.19
454	289846.1	-4.09	-3.62
455	290150.5	-3.42	-2.63
456	290449.2	-3.69	-3.17
457	290741.9	-2.99	-0.21
458	291028.7	-2.74	-1.96
459	291309.4	-2.04	1.59
460	291584.0	-2.38	0.76
461	291852.2	-2.87	-1.07
462	292114.2	-2.73	-1
463	292369.6	-2.2	-0.39
464	292618.8	-2.16	-0.62
465	292861.6	-4.04	-2.72
466	293098.3	-3.26	-2.21
467	293328.9	-2.7	-1.68
468	293553.6	-3.05	-1.59
469	293772.4	-2.93	-1.13
470	293985.4	-2.53	-0.57
471	294192.8	-2.38	-1.77
472	294394.6	-2.64	-1.56
473	294590.9	-2.92	-0.24
474	294781.9	-2.44	-0.28

475	294967.6	-3.2	-1.5
476	295148.1	-3.97	-3.07
477	295323.5	-3.46	-3.95
478	295494.0	-3.53	-2.92
479	295659.6	-3.52	-2.53
480	295820.5	-4.04	-2.93
481	295976.6	-3.91	-3.34
482	296128.2	-3.53	-3.45
483	296275.4	-3.25	-2.94
484	296418.1	-4.43	-4.59
485	296556.6	-4.38	-4
486	296690.9	-4.62	-4.38
487	296821.1	-5.63	-4.63
488	296947.4	-4.3	-4.41
489	297069.8	-3.66	-3.68
490	297188.4	-3.33	-3.98
492	297414.7	-4.51	-4.68
493	297522.6	-4.06	-3.72
494	297627.1	-3.81	-3.7
496	297826.3	-3.47	-3.48
497	297921.3	-3.45	-4.13
499	298102.4	-4.32	-3.99
500	298188.8	-4.69	-4.74
501	298272.4	-3.99	-3.93
502	298353.5	-4.24	-4.41
503	298432.1	-4.05	-4.65
504	298508.3	-4.32	-3.5
505	298582.2	-4.72	-3.94
506	298654.0	-4.43	-2.78
507	298723.6	-4.18	-1.66
508	298791.3	-3.69	-2.25
509	298857.1	-3.86	-1.78
510	298921.2	-4.49	-2.81
511	298983.5	-2.93	-2.2
512	299044.2	-3.83	-1.5
513	299103.5	-3.62	-2.22
514	299161.4	-4.85	-3.63
515	299218.0	-4.01	-3.85
516	299273.4	-3.57	-5.45
517	299327.7	-4.32	-5.66
518	299381.1	-5.15	-5.3

519	299433.5	-4.57	-5.02
520	299485.2	-3.75	-3.96
521	299536.1	-3.18	-2.95
522	299586.5	-3.93	-4.55
523	299636.4	-4.46	-4.67
524	299685.9	-4.74	-5.31
525	299735.1	-3.61	-3.83
526	299784.2	-3.18	-1.59
527	299833.1	-1.99	-0.11
528	299882.0	-2.35	-2.2
529	299931.1	-3.28	-4.45
530	299980.4	-2.66	-5
531	300029.9	-3.09	-5.15
532	300079.8	-2.77	-3.72
533	300130.2	-2.76	-4.74
534	300181.0	-2.82	-4.56
535	300232.4	-2.92	-4.37
536	300284.4	-3.06	-5.37
537	300337.0	-3.54	-4.56
538	300390.4	-3.05	-4.03
539	300444.6	-3.31	-1.49
540	300499.5	-4.04	-2.69
541	300555.4	-3.64	-2.71
542	300612.3	-3.39	-3.3
543	300670.1	-2.58	-1.76
544	300729.1	-3.58	-2.26
545	300789.2	-2.96	-0.67
546	300850.4	-3.22	-0.79
547	300912.9	-4.32	-3.15
548	300976.8	-4.59	-4.7
549	301042.0	-3.93	-3.28
550	301108.6	-3.68	-4.06
551	301176.8	-3.87	-3.08
552	301246.4	-4.26	-2.56
553	301317.7	-3.06	-2.27
554	301390.7	-2.7	-0.35
555	301465.4	-3.52	-0.73
556	301541.8	-3.48	-0.62
557	301620.1	-2.74	-1.45
558	301700.3	-4.01	-2.2
559	301782.5	-3.72	-1.61

560	301866.7	-3.55	-3.13
561	301953.0	-3.81	-3.78
562	302041.4	-4.46	-5.02
563	302132.1	-3.58	-4.9
564	302224.9	-3.96	-5.41
565	302320.1	-4.98	-5.11
566	302417.7	-4.66	-5.75
567	302517.7	-4.2	-5.9
568	302620.2	-4.08	-5.65
569	302725.3	-4.07	-2.7
570	302833.0	-4.34	-3.12
571	302943.3	-4.82	-3.48
572	303056.4	-4.22	-2.65
573	303172.3	-3.38	-3.39
574	303291.0	-4.16	-3.52
575	303412.6	-5.17	-3.88
576	303537.2	-3.47	-1.58
577	303664.9	-3.61	-1.14
578	303795.6	-4.3	-1.99
579	303929.5	-4.95	-4.48
580	304066.5	-4.57	-2.83
581	304206.9	-4.41	-3.23
582	304350.5	-4.55	-3.99
583	304497.5	-3.91	-2.77
584	304648.0	-4.02	-3.32
585	304802.0	-3.74	-3.26
586	304959.5	-3.38	-3.43
587	305120.7	-3.78	-4.42
588	305285.5	-4.98	-3.83
589	305454.1	-3.88	-4.17
590	305626.5	-4.41	-4.01
591	305802.7	-4.2	-4.56
592	305982.8	-4.77	-3.13
593	306167.0	-4.39	-2.36
594	306355.1	-5.01	-3.44
595	306547.3	-4.43	-3.92
596	306743.7	-4.5	-4.34
597	306944.3	-4.69	-3.56
598	307149.2	-4.33	-2.85
599	307358.4	-3.98	-2.85
600	307572.0	-3.18	-3.79

601	307790.0	-4.53	-3.21
602	308012.6	-3.95	-2.48
603	308239.7	-3.85	-2.63
604	308471.4	-2.93	-1.68
605	308707.8	-3.92	-0.87
606	308949.0	-4.17	-0.48
607	309194.9	-4.05	-1.95
608	309445.7	-4.15	-3.66
609	309701.5	-4.11	-1.45
610	309962.2	-4.99	-4.74
611	310228.0	-4.92	-2.45
612	310498.8	-4.35	-2.91
613	310774.8	-4.23	-3.21
614	311056.0	-4.27	-3.36
616	311634.4	-4.17	-3.66
617	311931.6	-3.68	-1.27
618	312234.3	-3.24	0.03
619	312542.5	-4.08	-2.36
620	312856.2	-4.16	-2.82
621	313175.6	-4.29	-4.33
622	313500.7	-3.98	-4.22
623	313831.5	-5.01	-1.77
624	314168.2	-4.83	-1.9
625	314510.7	-4.63	-1.03
626	314859.1	-5.35	-2.09
627	315213.5	-4.79	-1.49
628	315573.9	-4.52	-2.35
629	315940.5	-4.9	-4.25
630	316313.2	-5.28	-4.41
631	316692.2	-4.78	-4.4
632	317077.4	-4.99	-4.53
633	317468.9	-4.34	-2.37
634	317866.9	-4.26	-2.99
635	318271.3	-4.45	-2.55
636	318682.2	-4.01	-2.37
637	319099.7	-4.44	-0.93
638	319523.9	-4.16	-1.06
639	319954.7	-4.09	-1.66
640	320392.3	-3.76	-0.98
641	320836.7	-3.96	-1.2
642	321288.0	-4.38	-0.58

643	321746.2	-4.92	-1.59
644	322211.4	-4.8	-1.97